The Pennsylvania State University

The Graduate School

College of Engineering

SHEAR STRESS AND PARTICLE REMOVAL MEASUREMENTS OF A ROUND TURBULENT AIR JET IMPINGING NORMALLY UPON A PLANAR WALL

A Thesis in

Mechanical Engineering

by

Ryan M. Young

© 2013 Ryan M. Young

Submitted in Partial Fulfillment
of the Requirements
for the Degree of

Master of Science

May 2013

The thesis of Ryan M. Young was reviewed and approved* by the following:

Gary S. Settles
Professor of Mechanical Engineering
Thesis Advisor

Gita Talmage
Professor of Mechanical Engineering

Karen A. Thole
Professor and Head of Mechanical and Nuclear Engineering

*signatures are on file in the Graduate School

ABSTRACT

When a round jet of air impinges normally upon a wall, it imposes a shear stress parallel to the wall with radial symmetry from the impingement point. Particle removal from that surface is assumed to be mainly due to the imposed shear stress. This shear stress has been difficult to measure directly and has, in the past, been inferred from particle removal rates. Here we make a fundamental measurement of the mean shear stress imposed upon a planar wall by a normally-impinging turbulent air jet using the technique of oil-film interferometry. The resulting shear-stress distribution is then compared with measured removal rates of latex microspheres from a planar glass surface as a function of the radial distance from jet impingement normalized by the height of the nozzle exit above the surface. The particle removal experiments are carried out in quasi-steady flow with sparse (few collisions) particle distributions. These experiments show that the efficiency of particle removal is directly but not linearly related to the imposed shear stress. A distinct shear stress threshold was found, below which little or no particle removal occurred.

TABLE OF CONTENTS

LIST OF FIGURES

NOMENCLATURE

D	nozzle diameter, mm
H	jet standoff distance, mm
h	oil thickness, µm
N	fringe number from leading edge of oil
N_{after}	Number of particles after shear stress is applied
N_{before}	Number of particles before shear stress is applied
n_a	refractive index of air
n_o	refractive index of oil
r	radial distance from jet impingement point, mm
r_0	radial distance from jet impingement point to leading edge of oil-film, mm
P_{atm}	Atmospheric pressure, kPa
P_{jet}	Jet exit stagnation pressure, kPa
Re_o	Reynolds number at jet exit based on exit diameter
t	duration of jet impingement, s
u_o	average jet exit velocity, m/s
θ_i	light incidence angle, degrees
λ	wavelength of illumination, nm
μ_o	viscosity of oil, cs
ρ_a	density of air, kg/m^3
τ	shear stress, Pa
τ_{cr}	Critical shear stress, Pa
τ_{max}	theoretical/experimental maximum shear stress, Pa

Chapter 1

INTRODUCTION

1.1 Importance of Particle Removal

Impinging turbulent air jets are used for a wide range of particle removal applications. Jet impingement introduces a non-intrusive way to liberate particles from a surface. This is especially important when attempting to remove particles from a human subject. Frequently, this is the case for standoff chemical and explosive trace detection systems [1, 2, 3, 4]. In addition to trace detection, particle removal by air jets is common in the clean room and microelectronic industry [5, 6, 7]. Particle removal from these surfaces is assumed to be mainly due to the imposed shear stress. Therefore, it is important to characterize the shear stress for given standoff distances and jet conditions, such as jet stagnation pressure and nozzle diameter. With this characterization, a criterion can be determined for the effective radius of a particular process.

1.2 Shear Stress Profile

The shear stress profile produced by a normally-impinging round jet was previously determined by analyzing the removal rates of monodisperse particles on a smooth glass surface [8, 9]. These authors introduced the idea that such particles could behave as shear stress sensors. By knowing the jet conditions (jet standoff distance, nozzle diameter, and P_{jet}/P_{atm}), and determining the size of the particle removal path created by sweeping a normally-impinging jet over a uniform particle distribution, a shear stress profile could thus be obtained. However, this technique has limitations,

including an inability to account for the effect of particle impacts in dense particle distributions.

Oil-film interferometry (OFI) is an experimental method that utilizes the optical fringe pattern in a very-thin film of oil to directly determine mean wall shear stress. The shear stress at each interference fringe location can be derived from the measured slope of the oil film. Tanner and Blows [10] were the first to derive the theory of shear stress measurement from oil fringe patterns, while Driver [11] and Naughton [12] further developed this technique toward its present state of refinement for high-quality measurements of wall shear stress.

1.3 Particle Removal/Resuspension

Many studies have been performed on the removal or resuspension of particles in turbulent flows. Reviews by Ziskind et al. [13, 14] and Nicholson [15] attempt to synthesize an overall perspective from these many varied contributions. Fromentin [16], for example, removed particles from a plate in a wind tunnel, where removal was measured as a resuspended mass flux per unit time and unit surface area. Ibrahim et al. [17] performed a study in which microspheres were removed from a smooth glass surface during an accelerated turbulent flow caused by wind-tunnel startup. Their results indicate that the surface energy of adhesion and the microsphere radius are the primary factors in particle removal. Braaten et al. [18] also performed several experiments in a wind tunnel, and concluded that particles were removed based on discrete events such as velocity fluctuations or "bursts" within the boundary layer. Such bursts were earlier described by Corino and Brodkey [19] and Yung et al. [20].

From these and many similar studies of particle resuspension, a traditional aerodynamic model of the process was developed: Initially, a lift force related to the imposed aerodynamic shear stress was thought to act against the combined forces of particle adhesion to a surface. When adhesion is overcome, resuspension of the particle occurs. This traditional view has been modified by investigators such as Reeks and Hall [21], who proposed a *rock'n roll* model of particle detachment: Instead of leaping from the surface into the surrounding fluid due to a lift force, particles can rock or rotate about their attachment points until they eventually detach and roll off along the surface in the downwind direction.

This raises the possibility of a different particle resuspension mechanism due to impact by a particle rolling along the surface from upstream [14, 22, 23]. It is clear from these studies that such particle impacts, when they occur, are a more-robust mechanism for resuspension than aerodynamic forces alone.

Based on the above literature, two observations are made which motivate the present contribution to this field:

1) In many cases, resuspension experiments were done in uniform wind-tunnel-like flows where the aerodynamic shear stress τ imposed upon the surface was known or easily determined. Only a few studies [8, 9, 22, 24] considered resuspension due to gas-jet impingement upon a particle-bearing surface. Such impinging jets have important practical uses in particle removal, but the shear stress they impose on surfaces is not yet well-defined. In experiments performed in the Penn State Gas Dynamics Laboratory, short-burst air jets from round nozzles were impinged upon human subjects whose clothing was contaminated with 10-micron-range trace particles of cyclotrimethylene-

trinitramine (RDX). Dislodged particles were collected and the amount detected is shown in figure 1.1. Particles were dislodged by a number of mechanisms including shear stress, jet impact, and ruffling of clothing. However, jet impingement has become the principle means of liberating particles from people in a reasonably nonintrusive manner. Because the nozzle standoff distance was constant and the nozzle exit was sonic, it is understandable that the mass of detected RDX increased quasilinearly with jet stagnation pressure. Since jet momentum is conserved, an increase in stagnation pressure thus produces a proportional increase in jet momentum, which is thought to be responsible for particle removal from clothing [25, 26].

2) The majority of published resuspension experiments took no account of the density of particles applied to surfaces prior to testing, or of the potential for impact-induced resuspension by particles rolling along the surface. (Exceptions include [17, 23, 27, 28, 29], who tested near the leading edge of a deposited particle field in order to eliminate particle impacts from upstream). Resuspension models, on the other hand, generally consider individual particles rather than particle distributions, and especially not dense particle distributions. There apparently exists no definition of what constitutes a sparse vs. a dense particle distribution in this regard.

With these observations in mind, the goals of the present research are to measure the surface shear stress profile of a normally-impinging axisymmetric air jet from first principles using oil-film interferometry, and to correlate these data in terms of a non-dimensional shear stress profile. Then, the knowledge of this profile is used to explore the effect of the initial particle distribution density upon particle removal efficiency.

Finally a sparse particle distribution – wherein particles react to the applied aerodynamic shear stress independently of other particles – is used to examine the resuspension rate as a function of the aerodynamic shear stress.

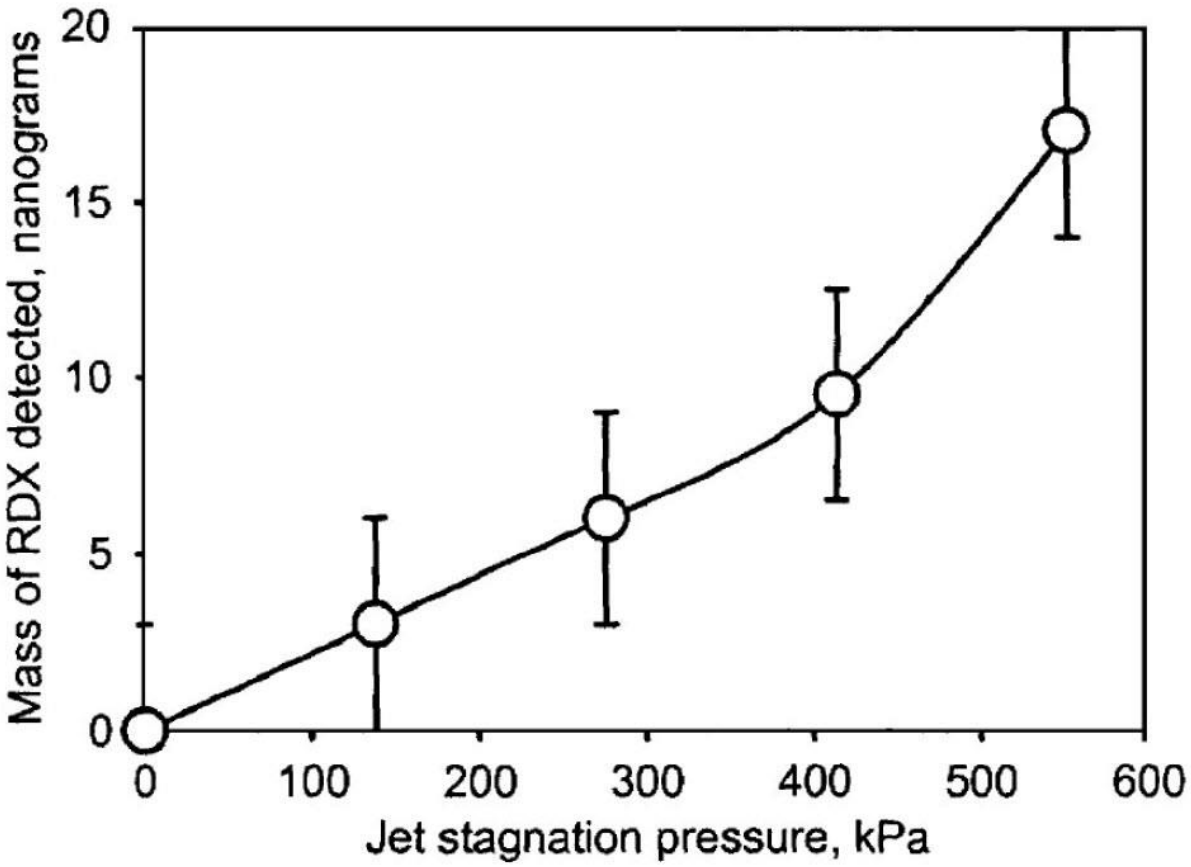

Figure 1.1: Mass of RDX removed and detected from human clothing as a function of jet stagnation pressure [18].

Chapter 2

SHEAR STRESS MEASUREMENTS

2.1 Oil-Film Interferometry

The experimental setup used here is shown schematically in Figure 2.1. A sodium-ion arc lamp with two distinct wavelengths of 589 and 589.6 nm was the illumination source. The light was diffused by ground glass to provide uniform illumination and reduce glare, and was directed at a 60 degree angle of incidence, θ_i, to the test surface.

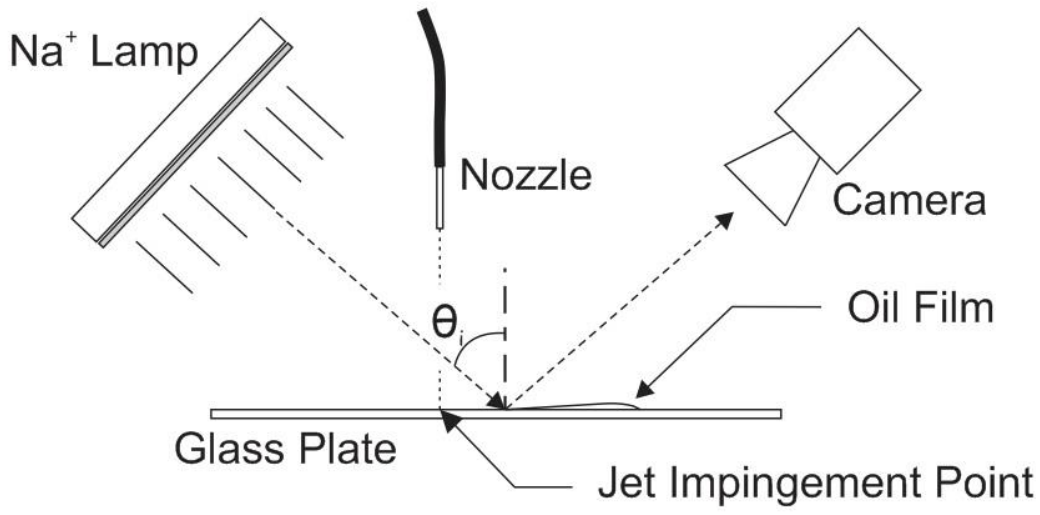

Figure 2.1: Schematic of the OFI setup

The shear stress measurements were performed on a 0.25 cm thick by 25 cm square polished glass plate test surface. Dow Corning 200 Fluid (μ_o= 50 cs at 25^0C) was chosen for the oil film because of its ability to maintain a consistent viscosity at varying temperatures. The oil temperature was held at 22.5^0C ± 2.5^0C, corresponding to an

average oil viscosity of 51 ± 1 cs. Thus, the oil viscosity remained within ±2% for all present experiments.

A compressed-air cylinder with a flow regulator fed dry air to a straight tubular nozzle (ID=3.75 mm) to produce the impinging jet. A Nikon D80 digital SLR camera captured still images of the oil-film experiments at 12 megapixel resolution.

2.2 Impinging Jet Setup

Round free jets, such as those produced here, are considered to have fully-developed velocity profiles at a distance of 8 nozzle diameters downstream of the nozzle exit [2]. For the present study, only fully-developed round jet impingements were considered, and the minimum standoff distance (distance from nozzle exit to plate surface) for these experiments was determined accordingly. The standoff distance was thus varied between 6 cm (H/D=16) and 7.5 cm (H/D=20) for these tests. The straight-walled tubular nozzle used here is shown in Figure 2.2.

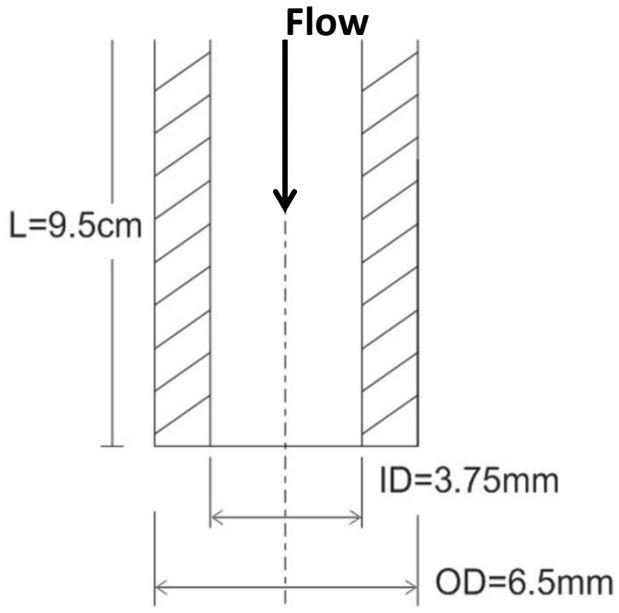

Figure 2.2: Straight nozzle dimensions

The jet stagnation pressure was varied independently using a pressure regulator and precise pressure gauge attached to the compressed air source. Data were recorded for both subsonic and sonic jet exit conditions. A plenum chamber was used in order to stabilize the stagnation pressure during testing. This resulted in a variation of no more than ± 3.4 kPa in the stagnation pressure. The subsonic data were taken for a stagnation pressure ratio P_{jet}/P_{atm} of 1.11 ± 0.04, which yielded an average exit velocity of 136 m/s and an exit Reynolds number (Re_o) of $3.3x10^4$ for an air temperature of 296 K. Sonic-nozzle-exit data were taken for P_{jet}/P_{atm}=2.52 ± 0.04, which produced underexpanded flow and shock diamonds after the flow exited the nozzle.

2.3 Oil-Film-Interferometry Imaging and Processing

A calibration image is recorded for each experiment to convert pixel dimensions to radial distances from jet impingement. Each test begins by placing a drop of oil on the glass plate at the jet impingement point. The air jet is then turned on and is run continuously until a clear interference fringe pattern forms around the impingement point, as shown in Figure 2.3. An image is taken of this pattern and processed to determine the pixel value of the ring center, which is the jet impingement point (r = 0). The glass is then cleaned and an oil-film with a straight leading edge is placed beside the impingement point. This oil-film is created by first placing a drop of oil on the glass, then smearing the oil with a razor blade, thus providing an approximately-zero oil thickness at the film leading edge. (The location of zero oil thickness is required to subsequently determine the oil thickness at each of the fringe locations.) The air jet is then turned on continuously and an image of the oil-film interference pattern on the glass is taken every ten seconds. Figure 2.4 shows a typical image of the interference pattern in the oil-film

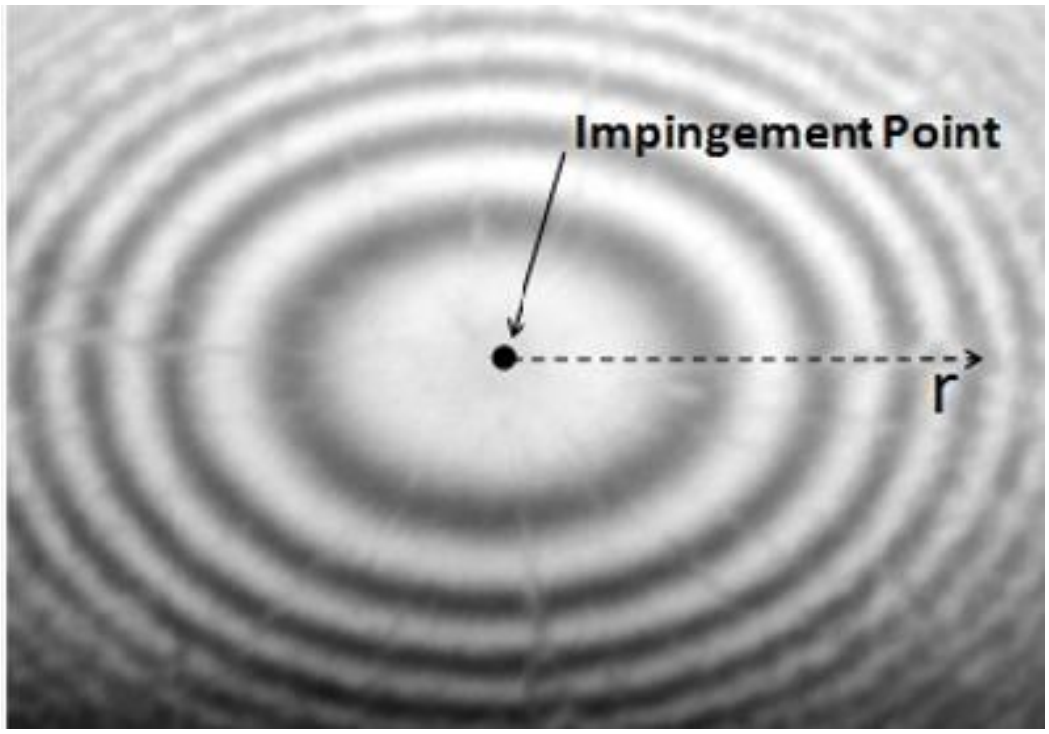

Figure 2.3: Concentric interference fringes observed when oil drop is placed at impingement point

with its straight leading edge at the left.

Each recorded image is converted to grayscale and a plot of pixel intensity versus pixel number along the radius of the jet impingement is obtained using MATLAB (Figure 2.5). Each maximum and minimum in Figure 2.5 marks the center of a bright fringe and a dark fringe, respectively. The height of the oil at each of these points can be determined according to Naughton and Liu [30] using:

$$h = \frac{N\lambda}{4}\left(\frac{1}{\sqrt{n_o^2 - n_a^2 sin^2\theta_i}}\right) \quad (1)$$

Knowing the oil height h at each fringe location allows h to be expressed as a function of the radial distance (r) from the impingement point. The shear stress can then be found according to Tanner and Blows [10],

$$\tau = \frac{2\mu_o}{th^2 r}\int_{r_0}^{r} hrdr \quad (2)$$

The calculation of τ is performed at each fringe location, integrating from r_0 to the radial distance, r, of the fringe in question.

2.4 Experimental Results

The first experiments were performed with a pressure ratio (P_{jet}/P_{atm}) of 1.11 ± 0.04, yielding a subsonic average nozzle exit velocity of 136 m/s. The shear stress profile was first determined for a jet standoff distance of 7.5 cm (H/D=20) using the setup described in Section 2.1. The jet standoff distance was then decreased to 6 cm (H/D=16) for the same jet exit condition, which increased the maximum shear stress at the surface

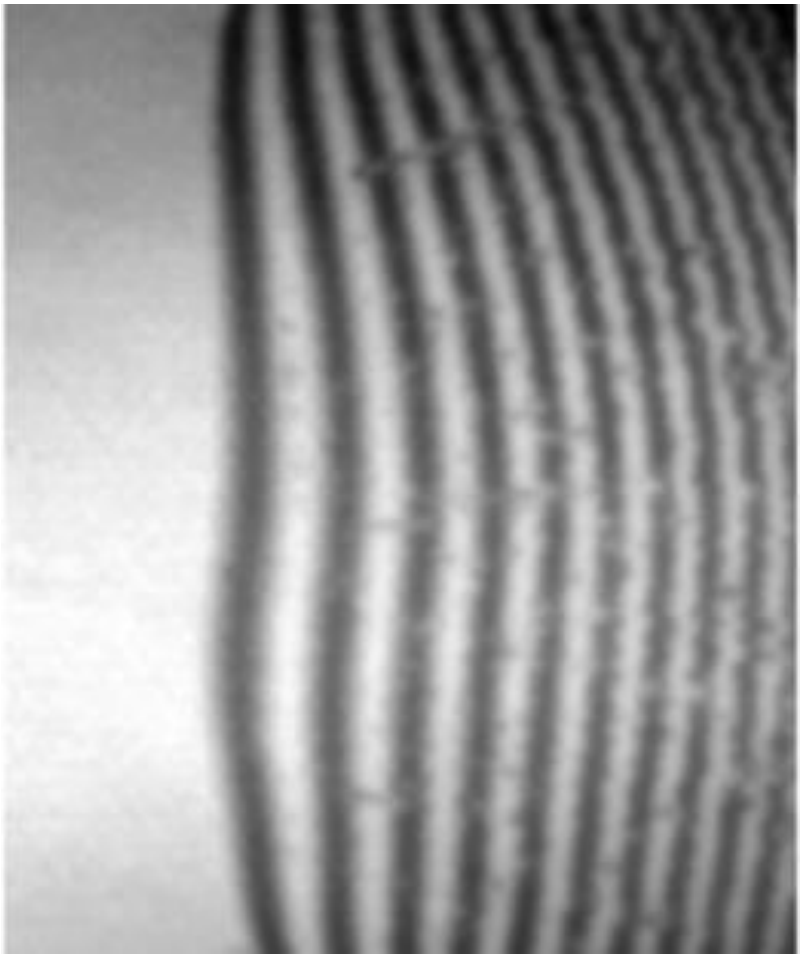

Figure 2.4: Fringe pattern in oil with leading edge

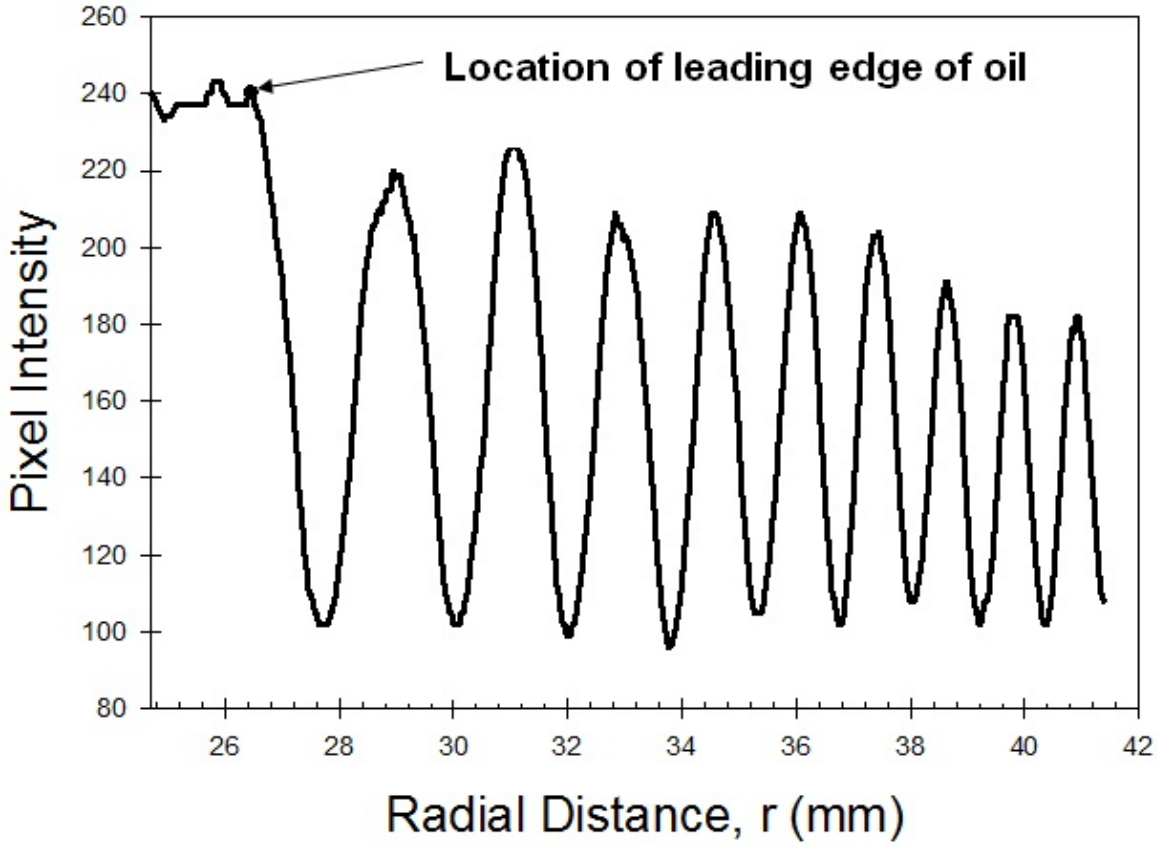

Figure 2.5: Pixel intensity vs. radial distance from impingement point

by about 15%. The measured shear stress as a function of radial distance from jet impingement for both of these nozzle standoff heights is plotted in Figure 2.6.

The data of Figure 2.6 can be non-dimensionalized to allow comparisons between experiments: The radial distance is normalized as r/H, and the shear stress is normalized as τ/τ_{max}, where τ_{max} is the theoretical maximum shear stress, which occurs at r/H = 0.09 as found by Phares, et al. [9]:

$$\tau_{max} = 44.6\rho u_o^2 Re_0^{-1/2} \left(\frac{H}{D}\right)^{-2} \quad (3)$$

The normalized data from Figure 2.6 are plotted in Figure 2.7, where it is observed that the normalization succeeds in collapsing the effect of varying nozzle standoff distance.

The present experimental results were compared to theoretical laminar boundary layer impingement-region behavior and the experimental results of Smedley, et al. [8], as shown in Figures 2.8 and 2.9. A laminar impingement region is used here, as also used by Smedley, et al. [8], because it was assumed that the strong favorable pressure gradient in the impingement region would cause a turbulent jet flow to re-laminarize. However, this assumption was not previously supported by observation. Based on a subsonic nozzle exit flow with a jet spreading half-angle of 12^0 [31], the jet-impingement region extends out to an r/H of 0.21 in Figure 2.8 and 2.9 (r/H = 0.21 corresponds to the jet radius at the location of the edge of the impingement on the plate.). The experimental results match the predicted shear stress from laminar-boundary-layer impingement-region theory quite well for $0 < r/H < 0.21$. This also appears to be the location beyond which the data from [8] no longer match the present OFI results in Figure 2.8.

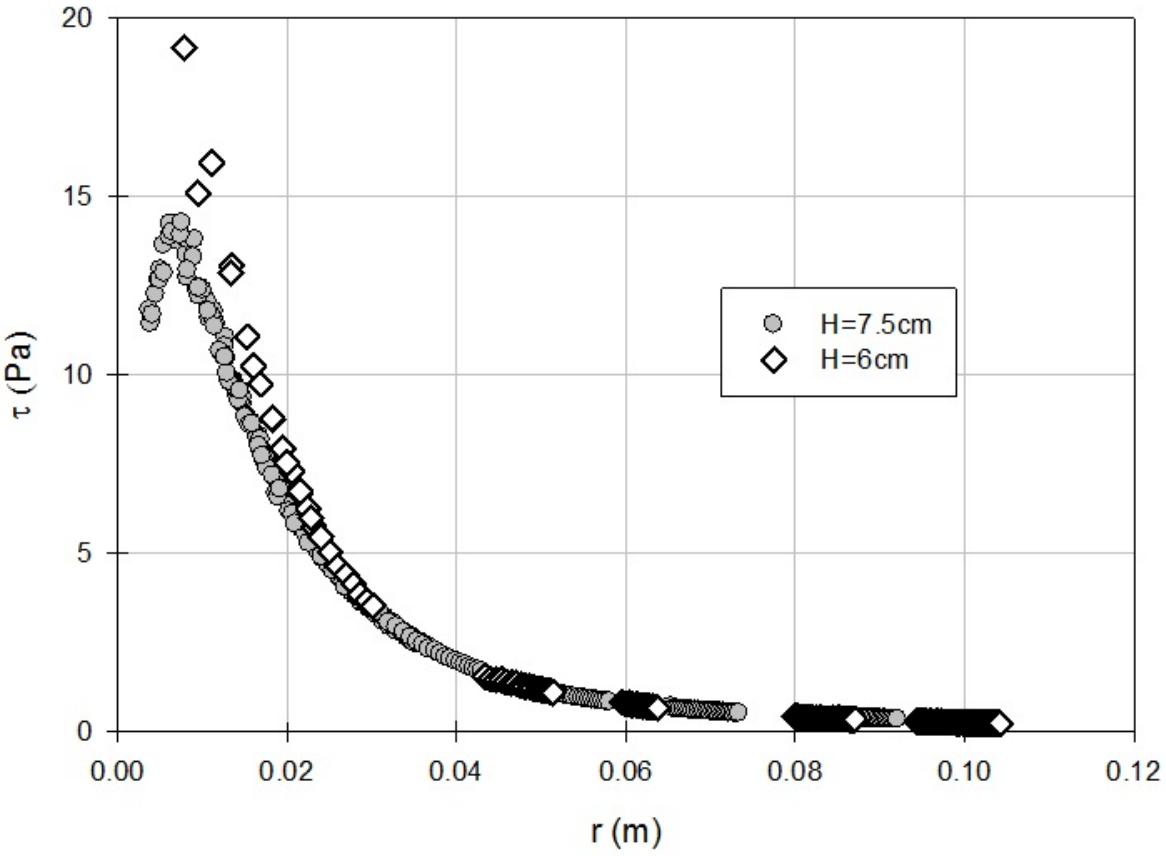

Figure 2.6: Shear stress profile for varying standoff distances for subsonic nozzle exit flow. Maximum error caused by impingement location uncertainty and oil viscosity changes due to temperature fluctuations is represented by the size of the symbols

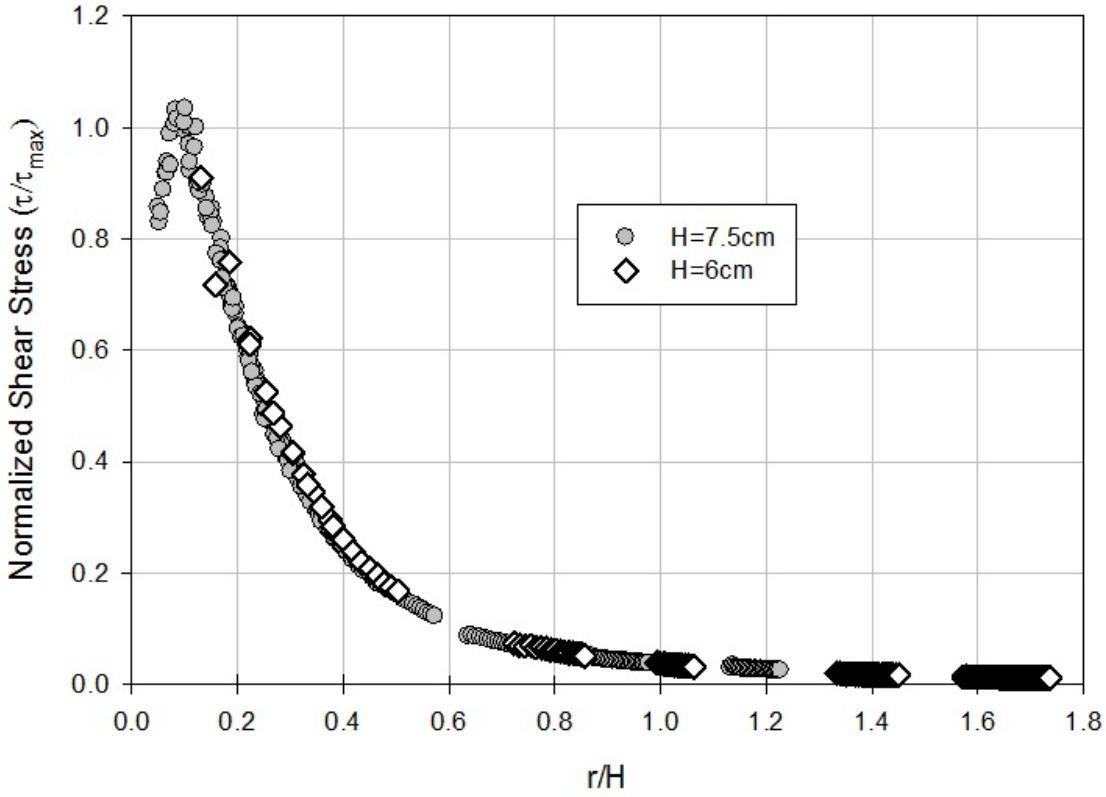

Figure 2.7: Normalized shear stress profile for varying standoff distances for subsonic nozzle exit flow

The comparison in Figure 2.8 between the present results and those of Smedley, et al. [8] is an important one that bears discussion. Smedley, et al. assumed that the impinging-jet wall shear stress distribution could be directly inferred from their measured particle removal data, whereas we have measured the mean wall shear stress directly without reference to particle removal. The similar behavior of the two datasets, revealed in Figure 2.8, indeed supports the widely-assumed traditional model of particle removal due to aerodynamic drag, but the comparison is not perfect. Outside the immediate jet-impingement zone, i.e. for $r/H > 0.21$, the present shear-stress data rapidly asymptote toward zero whilst the shear-stress-inferred-from-particle-removal data of Smedley, et al. [8] remain distinctly higher. The reason for this discrepancy is not known, but two important differences in the datasets of Figure 2.8 should be considered.

First, the dense particle distributions used by Smedley, et al. [8] to make their measurements likely involved a particle-impact resuspension mechanism as well as a mechanism based solely on the applied aerodynamic shear stress. Given a sufficiently-sparse particle distribution, however, this particle-impact mechanism should become negligible. This suggests that jet-impingement particle-removal experiments with sparse particle distributions are needed, and that approach is pursued in the next section of this thesis.

Second, the present OFI technique for wall shear-stress measurement has no effective frequency response, and thus yields only the mean shear stress. It does not reveal the fluctuating component of wall shear stress beneath a turbulent flow, e. g. due to turbulent bursts as mentioned in the Introduction. Consequently, actual particle

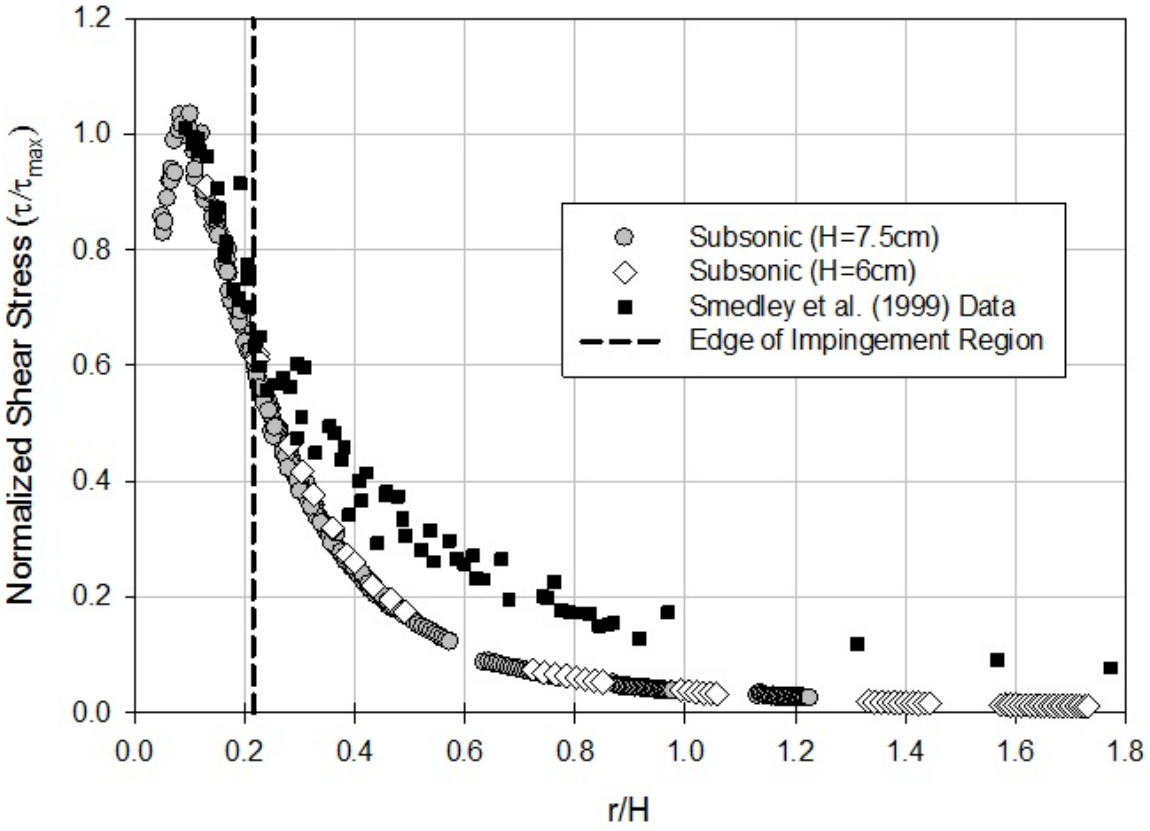

Figure 2.8: Present experimental shear stress profile for subsonic flow compared with data from Smedley et al. [8]

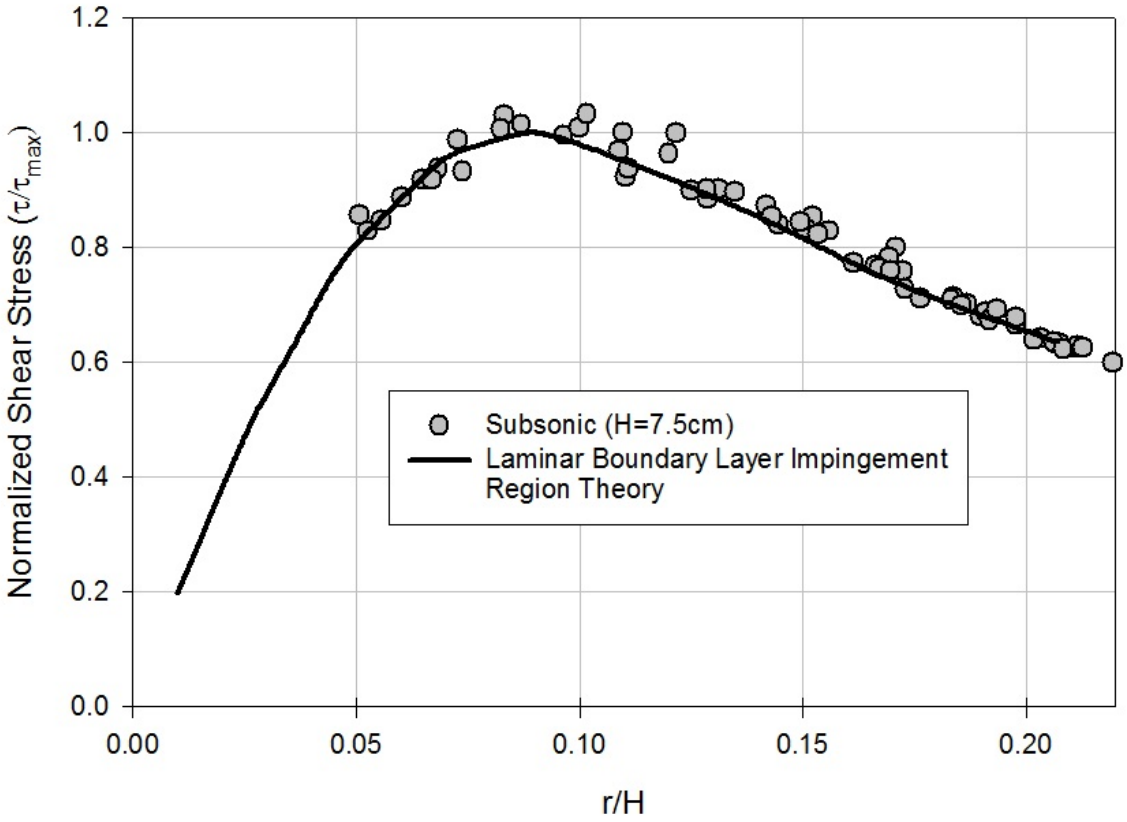

Figure 2.9: Present experimental shear stress profile for subsonic flow compared with the predicted shear stress profile based on laminar boundary layer theory for a circular jet [9] within the impingement region

resuspensions at the larger r/H values in Figure 2.8 may not tend toward zero as rapidly as does the mean shear stress measured here by OFI.

Further OFI data were acquired for sonic nozzle-exit conditions at nozzle standoff distances of 12 and 16.5 cm and at a pressure ratio (P_{jet}/P_{atm}) of 2.52 ± 0.04. For a straight nozzle with a sonic exit, shock diamonds are expected to occur at the exit of the nozzle. The sonic nozzle-exit condition was observed qualitatively using a z-type schlieren system as described by Settles [32]. A schematic of the setup is shown in Figure 2.10. This optical method allows normally-invisible changes in density in air to be readily seen. Because shock waves are an abrupt change in density, a schlieren setup makes them very visible. Figure 2.11 shows a schlieren image of the shock diamonds produced at the exit of the nozzle.

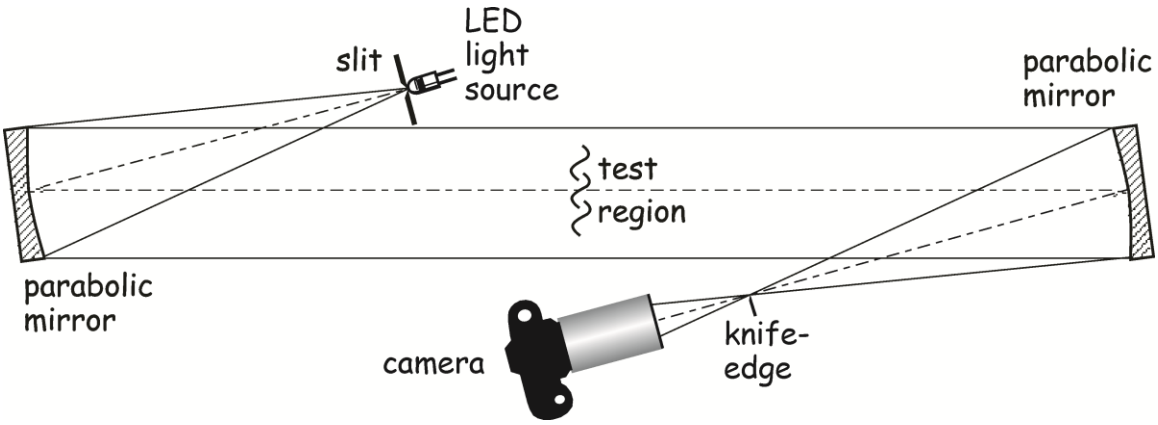

Figure 2.10: Schematic of the z-type schlieren setup used to view sonic nozzle-exit air flow

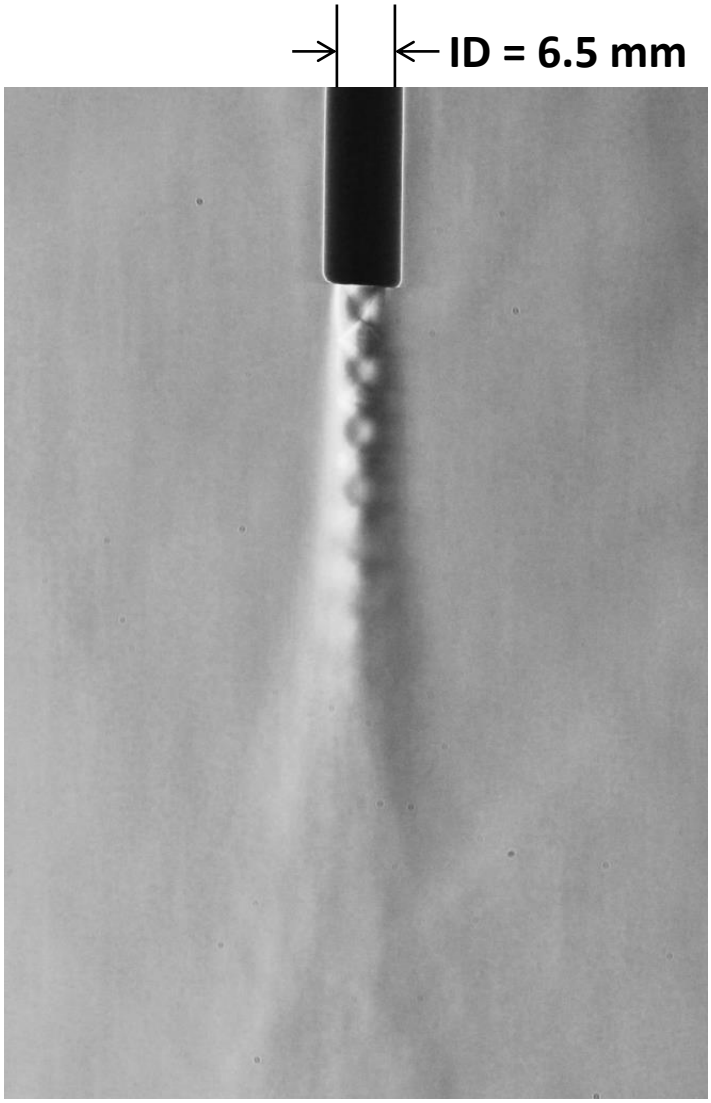

Figure 2.11: Schlieren image of a sonic nozzle-exit condition with visible shock diamonds

Figure 2.12 shows the shear stress data for the sonic-nozzle-exit experiments, where τ_{max} is now taken directly from the experimental maximum rather than a theoretical maximum, due to the complexity of the flow. (The theoretical solution no longer yields an accurate prediction of maximum shear stress based on initial jet conditions because the theoretical solution does not account for shock waves.)

The sonic-nozzle-exit data in Figure 2.12 reveal the same normalized shear stress profile as the subsonic data shown earlier. No correction was made to subtract the supersonic region from the jet standoff distance, even though shock diamonds are obviously present (Figure 2.11). This would not be the expected result, however, if a Laval nozzle was used in place of the present straight tubular nozzle with sonic exit.

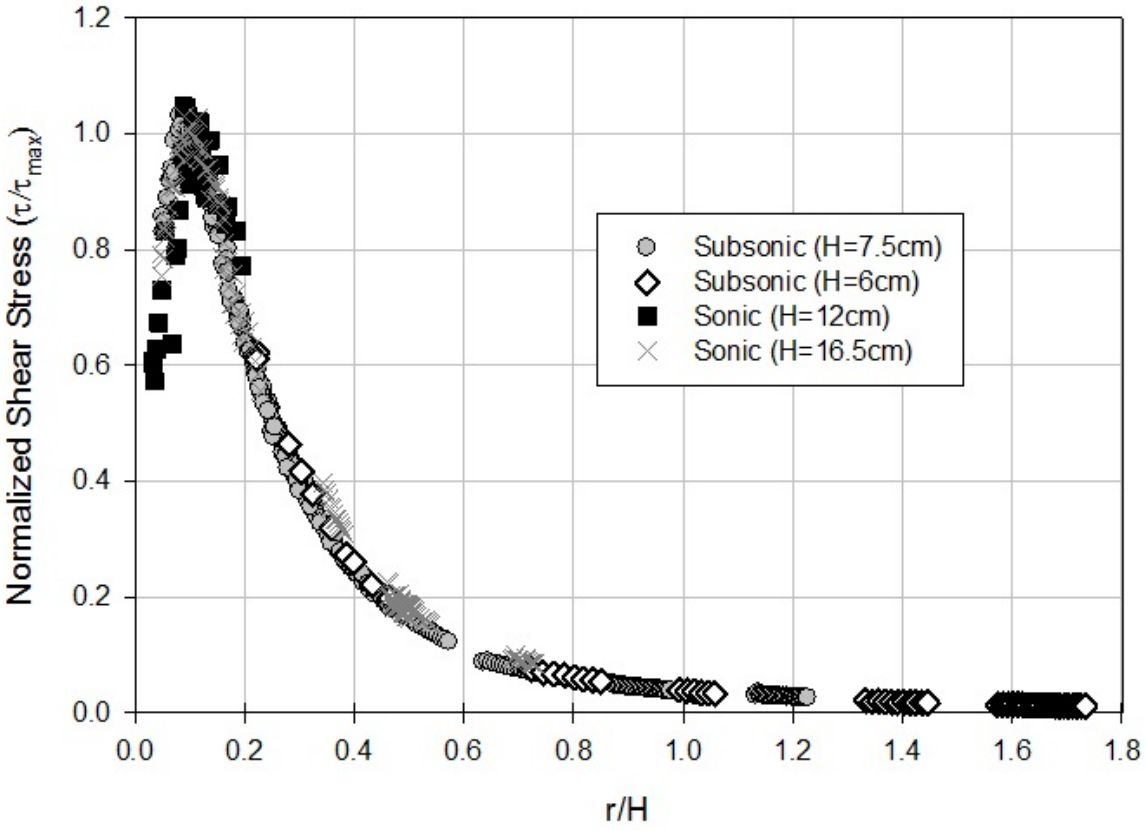

Figure 2.12: Normalized shear stress profile for varying standoff distances for subsonic and sonic jet exit flows. All data are normalized by the maximum shear stress, which is derived theoretically for subsonic exit flow and measured experimentally for sonic exit flow. Maximum error caused by impingement location determination and oil viscosity changes due to temperature fluctuation is represented by the size of the symbols.

Chapter 3

PARTICLE REMOVAL

3.1 Experimental Setup

The present experiments for determining particle removal efficiency used the same glass plate, nozzle, air tank, and regulator as in the OFI experiments just described. The exit pressure ratio, P_{jet}/P_{atm}, was 1.11 ± 0.04 (the same condition as the subsonic OFI tests). For these experiments, however, a pulsed air jet was used instead of a continuous one. A solenoid valve provided consistent jet pulse times of 0.02 seconds in these experiments.

The OFI data shown previously are steady-state measurements of wall shear stress distributions, since the OFI technique has essentially no frequency response. In order to use these results in understanding particle removal, steady-state removal data are required in principle. This, however, presents a challenge: if a steady jet impingement is applied to a surface with attached particles for an extended time period, all particles are resuspended and no useful measurement can be made. Instead, it was determined that if the nozzle standoff distance was increased to 150 mm, less than 100% particle removal would be achieved, even at the location of maximum mean wall shear stress, for air jet impingement under the current conditions (136 m/s nozzle exit speed) lasting only 0.02 seconds. During this interval it is important for steady-state conditions to be reached quickly and maintained, so a fast-acting solenoid valve was used to bring the jet flow up to steady operation in less than 1 ms. Quasi-steady-state flow was verified for at least 20 ms using a fast-response piezo-resistive pressure transducer to measure the first derivative of jet stagnation pressure versus time. Figure 3.1 shows the normalized output

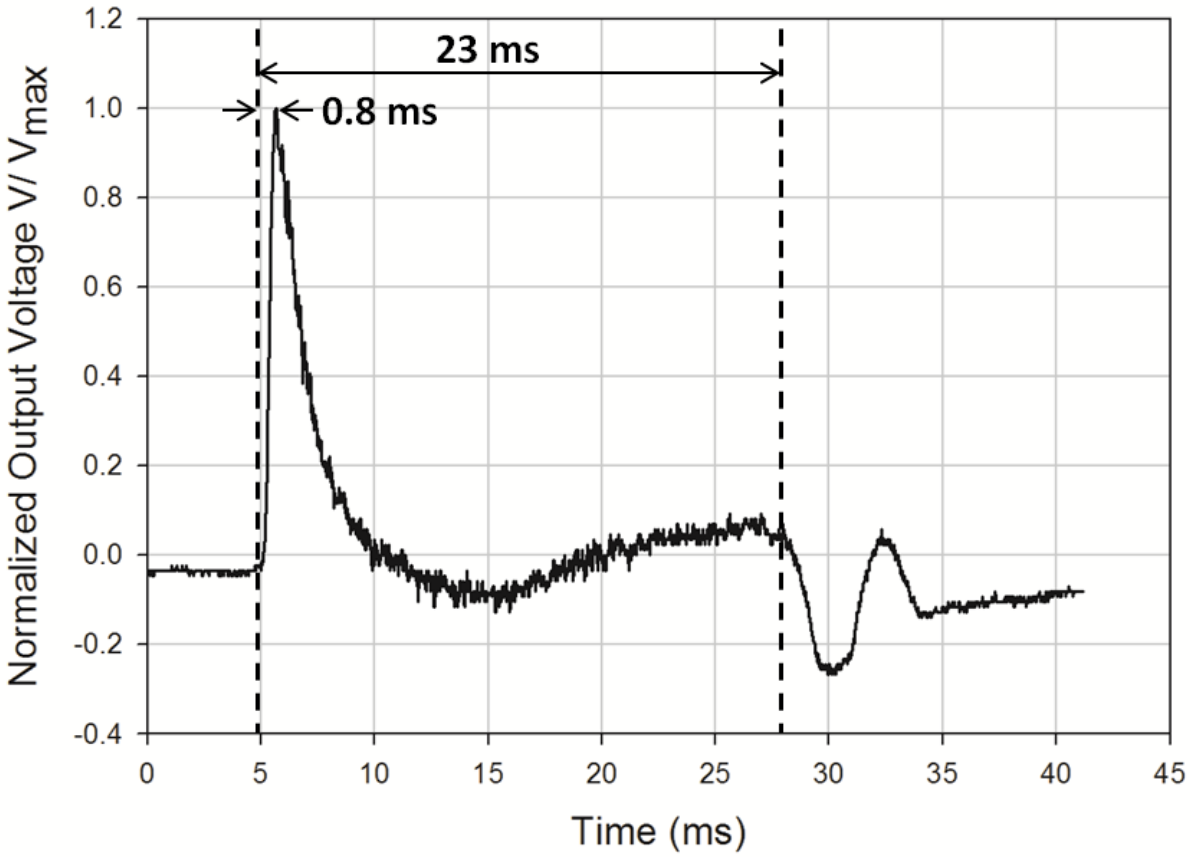

Figure 3.1: Normalized output voltage of the piezo-resistive pressure transducer used to determine the jet rise time and duration of constant pressure for the jet pulse used for particle removal experiments

voltage versus time for a single jet pulse. Because the piezo-resistive transducer can only measure changes in pressure, once a maximum pressure is achieved and the pressure remains constant, the transducer relaxes, and the output voltage returns to zero. Once the solenoid closes and the pressure on the transducer decreases, a negative voltage results. From Figure 3.1, it can be readily seen that the jet rise time is less than 1 ms, and the duration of constant pressure is slightly longer than the nominal 20 ms. In that time interval a fluid particle at the nozzle exit velocity would travel almost 20 times longer than the 150 mm standoff distance of the nozzle exit from the impingement plate.

Under these circumstances, it is determined that all particle resuspension experiments were performed under quasi-steady-state conditions. Thus, the measured steady-state OFI wall shear stress distribution is used to correlate the particle resuspension data.

Relative humidity was recorded for every test, and ranged from 20-55%. Within this range, identical experiments were performed at 22% and 52% relative humidity, with no change in particle removal observed.

The particles used in these experiments were Duke Scientific 31-μm-diameter red fluorescent latex microspheres. These particles were deposited on the glass surface using a "settling chamber," which allowed the particles to separate and settle in a consistent manner, creating a near-uniform distribution. The settling chamber consisted of a box with a nozzle inserted into the side and angled in the vertical direction. Particles were placed into one end of the nozzle and shot into the box by shooting air from a dust-off can into the nozzle. The particles were distributed in a narrow ~1 cm strip by using a barrier inside the box. The setup can be seen in Figure 3.2. This "strip" of particles was

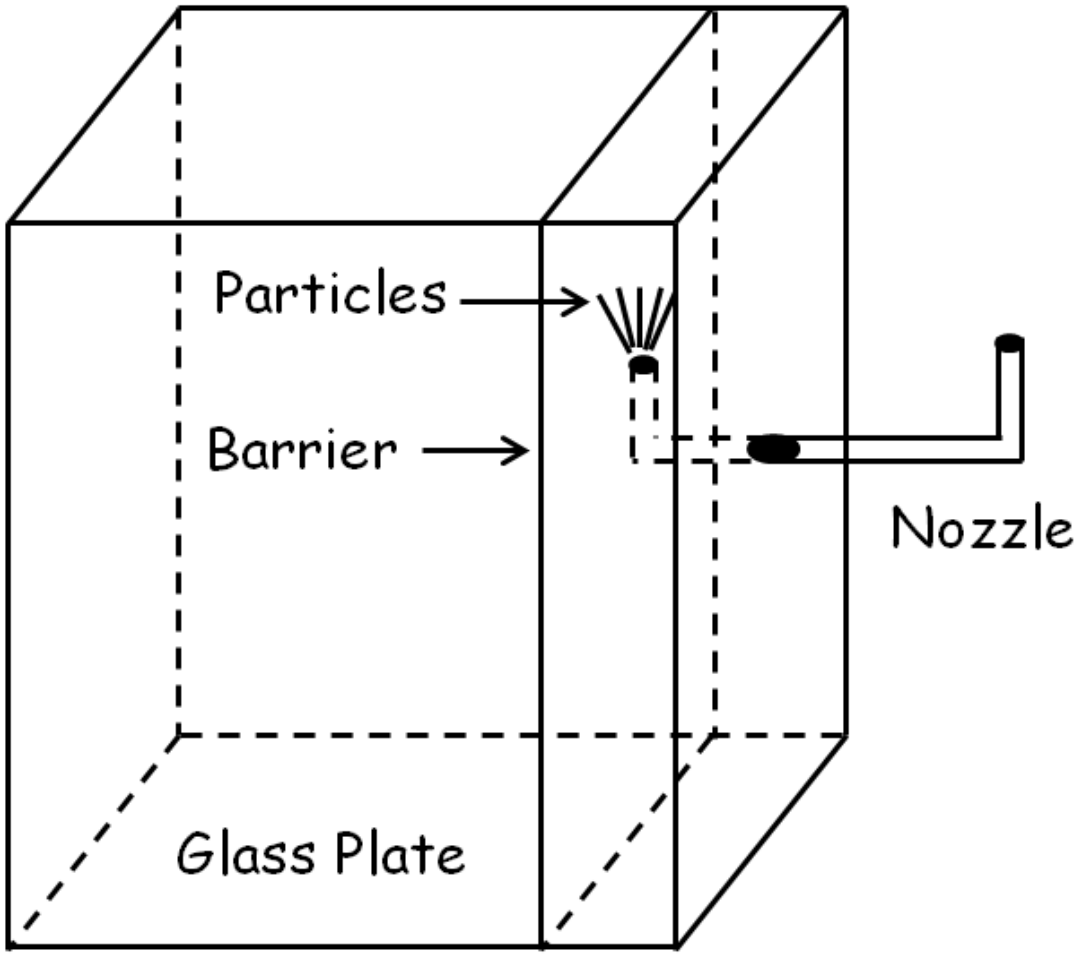

Figure 3.2: Schematic of the particle settling chamber

aligned perpendicular to the air flow. Only the leading edge of the particle distribution was interrogated, which eliminated the possibility of particles from outside the strip impacting and dislodging particles inside the field-of-view. Static-electric forces between particles and the glass plate were minimized by grounding the plate before and after applying the particles.

Imaging was done with a Photron FASTCAM APX high-speed digital video camera fitted with an Edmund Optics VZM™ 450I microscopic lens with a 3x zoom. The camera frame rate was 10,000 frames per second. It was positioned to image the particles from underneath the glass plate. A schematic of the entire setup is shown in Figure 3.3.

3.2 Image Processing

A MATLAB routine, included in the Appendix, was written to analyze the resulting particle resuspension images by counting individual particles within a certain field-of-view. This was used to determine the number of particles in the field-of- view on the glass surface before and after a 0.02 sec air-jet pulse. The routine also calculated the initial mean particle separation for each experiment, this being the average distance between a particle and its closest neighbor. This value is used to determine the effect of particle spacing on removal efficiency.

A particle removal efficiency index was then calculated as:

$$\text{Removal Efficiency} = \frac{N_{before} - N_{after}}{N_{before}} \quad (4)$$

The field-of-view for particle counting was chosen to be 6x6 mm, which contained enough particles for a proper statistical sample. A typical 6x6 mm region contained 75 particles in these experiments.

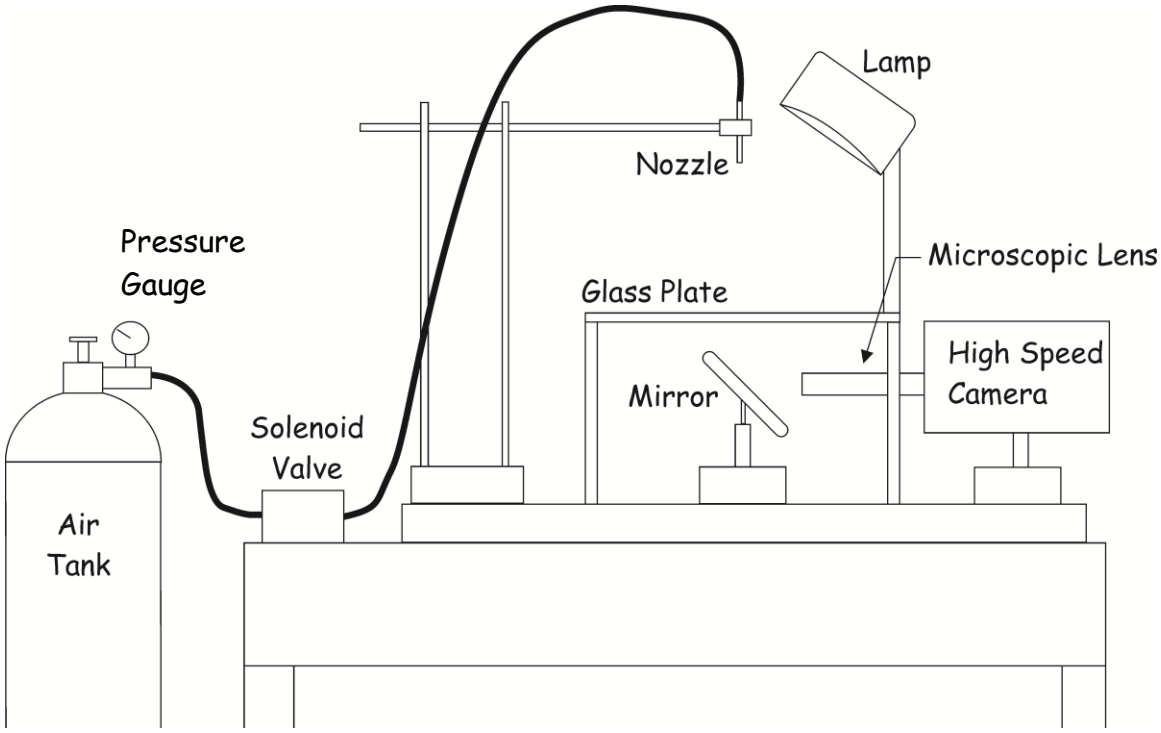

Figure 3.3: Schematic of the particle removal experimental setup

The MATLAB routine also created a histogram of the nearest-neighbor results. This test indicated if there were any irregularities in the distribution of particles that could lead to an untypical result.

3.3 Experimental Results

As discussed earlier, primary present interest is in the effect of particle spacing (i.e. the density of the applied particle distribution on the test surface) on jet-impingement-induced particle resuspension. Several high-speed, high-magnification videos were taken of air flows applied to high-density particle distributions. These distributions contained several particles already in contact with each other. There were also many particles upstream of the viewing field in order to observe, qualitatively, the effect this had on removal. A video demonstrating both of these effects was filmed at 75,000 frames per second. Figure 3.4 show the removal of particles due to collisions from upstream particles. Figure 3.5 show a particle that was not removed due to the interaction with a particle it was in contact with. These results generated an immediate concern over particle spacing and the effect it has on particle removal. It was apparent that tests must be performed for distributions where particle-particle interactions were minimal, if aerodynamic forces alone were to be held responsible for particle removal.

Due to particle interaction concerns, the mean particle spacing was calculated for every test. Results yielded an overall average spacing of 13.37 particle diameters (415 μm) with a standard deviation of 2.68 particle diameters. Furthermore, a histogram indicated the uniformity of the distribution. Ideally, all of the particle would be grouped around the average particle spacing. However, as would be expected, a number of particles settled in groups close to each other, and a few “lone” particles ended up a large

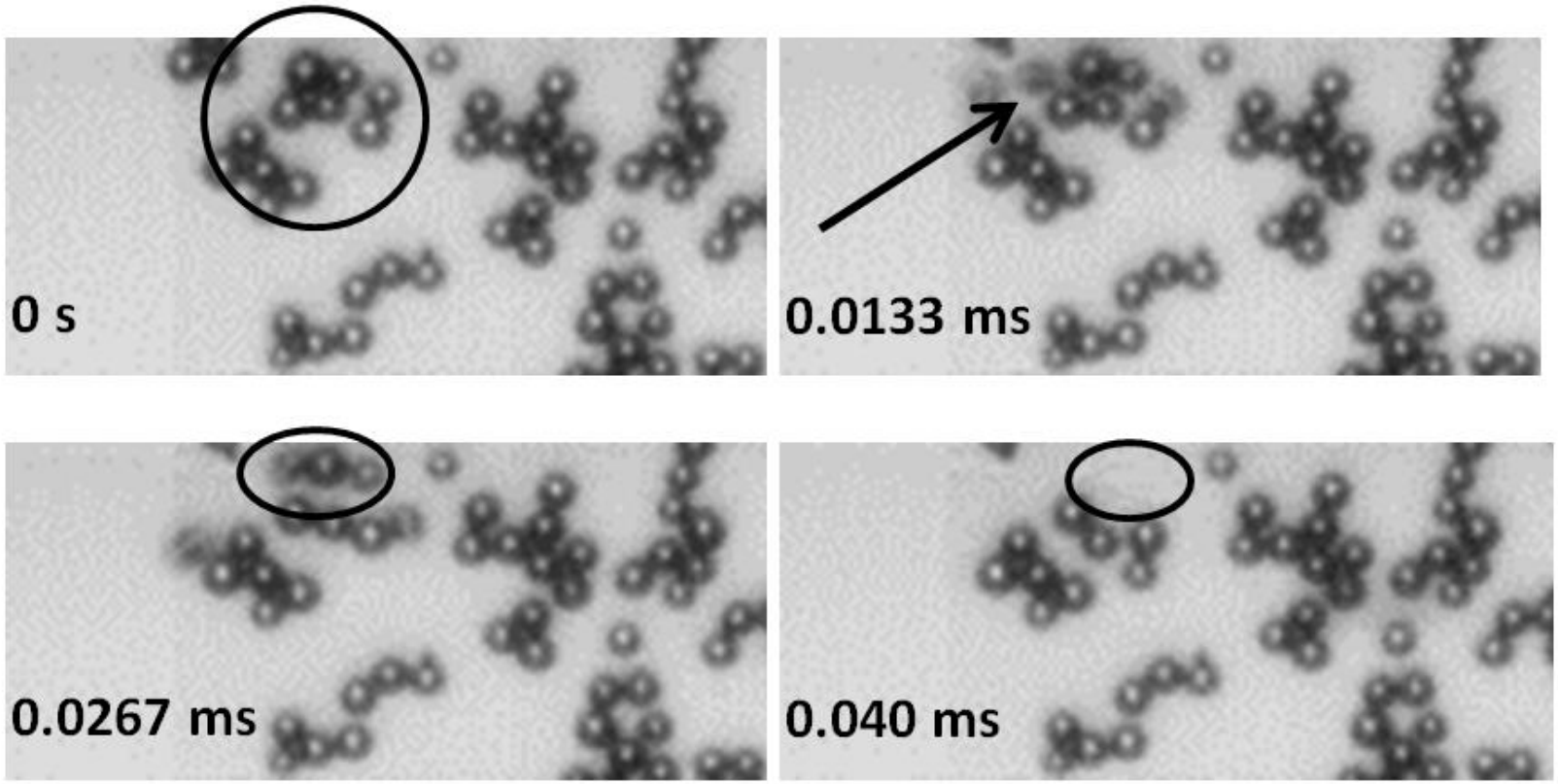

Figure 3.4: Frames from a high speed video (75,000 frames per second) showing the removal of particles in a dense particle field due to particle-particle collisions. Particle diameter is 31 μm

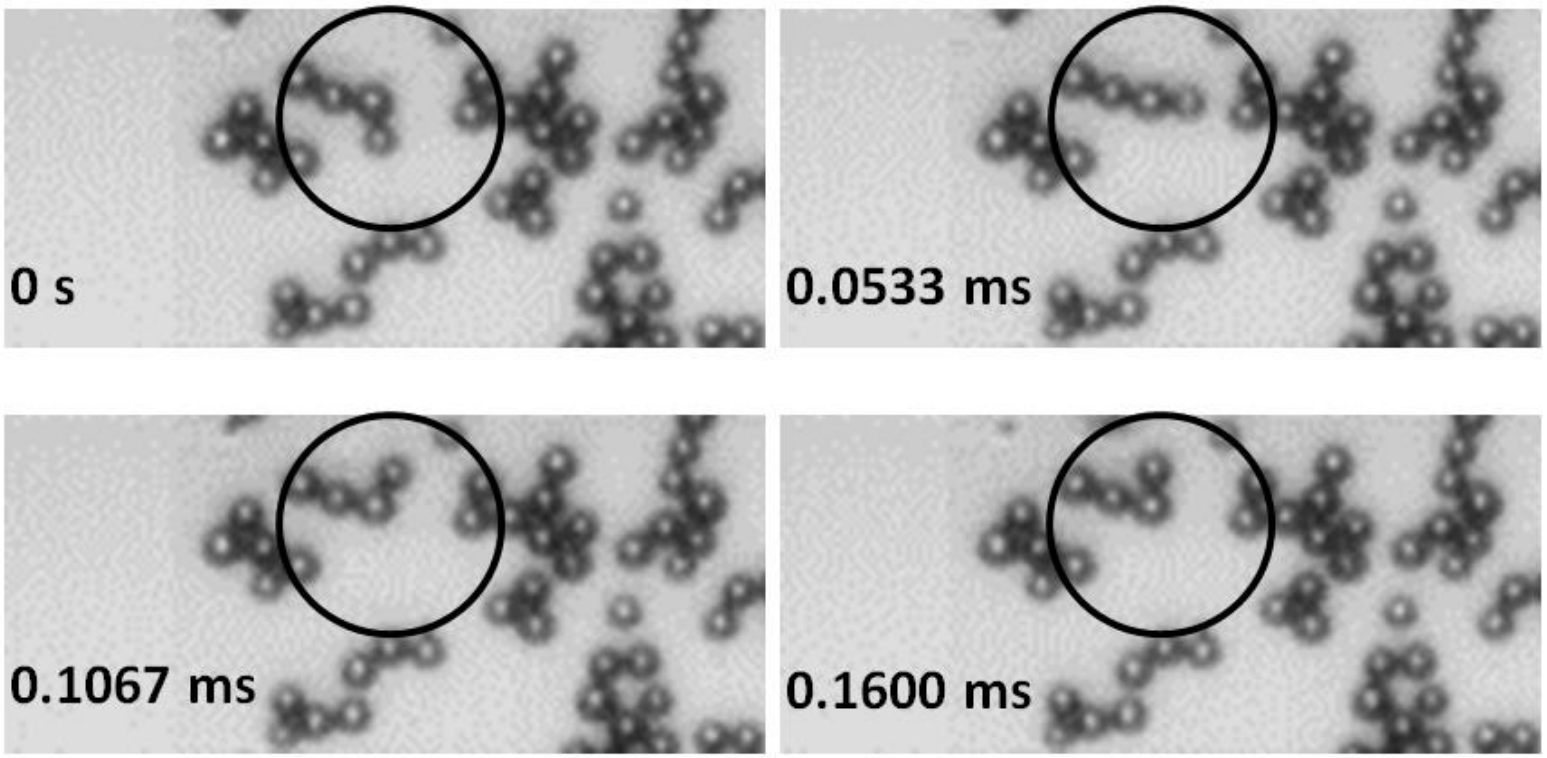

Figure 3.5: Frames from a high speed video (75,000 frames per second) showing the attachment of a particle to another in a dense particle field. Particle diameter is 31 μm

distance from the others. A typical distribution for a single test is shown in Figure 3.6, and the distribution for the entire data set for a jet standoff distance of 150 mm and a radial distance of 75 mm is shown in Figure 3.7.

In order to determine the effect of particle spacing on resuspension, several tests were performed at jet-impingement location r/H = 0.5 on the test plate while varying the mean particle spacing from about 5.6 to 21 particle diameters (174 – 651 μm). Figure 3.8 shows these results in terms of particle removal efficiency vs. mean particle spacing. For a particle spacing of 10 diameters and greater, the removal efficiency becomes effectively constant, i.e. it becomes effectively independent of particle spacing for such "sparse" particle distributions. A mean particle separation of 10 diameters and greater was required for data sets at other radial distances from the impingement point.

For particle spacing less than 10 particle diameters in Figure 3.8, the removal efficiency is a strong function of spacing. Here the distribution is "dense," although there is not an important difference with dense-distribution results in the literature, described earlier, where particle impacts play a commanding role. Here, despite the dense distribution, resuspension by particle impact has been essentially eliminated in the design of the experiment. This is an unknown regime of particle removal, and its proper investigation is unfortunately beyond the scope of this effort.

Further data were taken at various r/H values for jet impingement with the nozzle height set at 15 cm (H/D=40). The radial distance was varied by re-positioning the nozzle along a radius while keeping the camera focused on a single 6x6 mm region of the glass surface. The resulting data, shown in Figure 3.9, give particle removal efficiency as

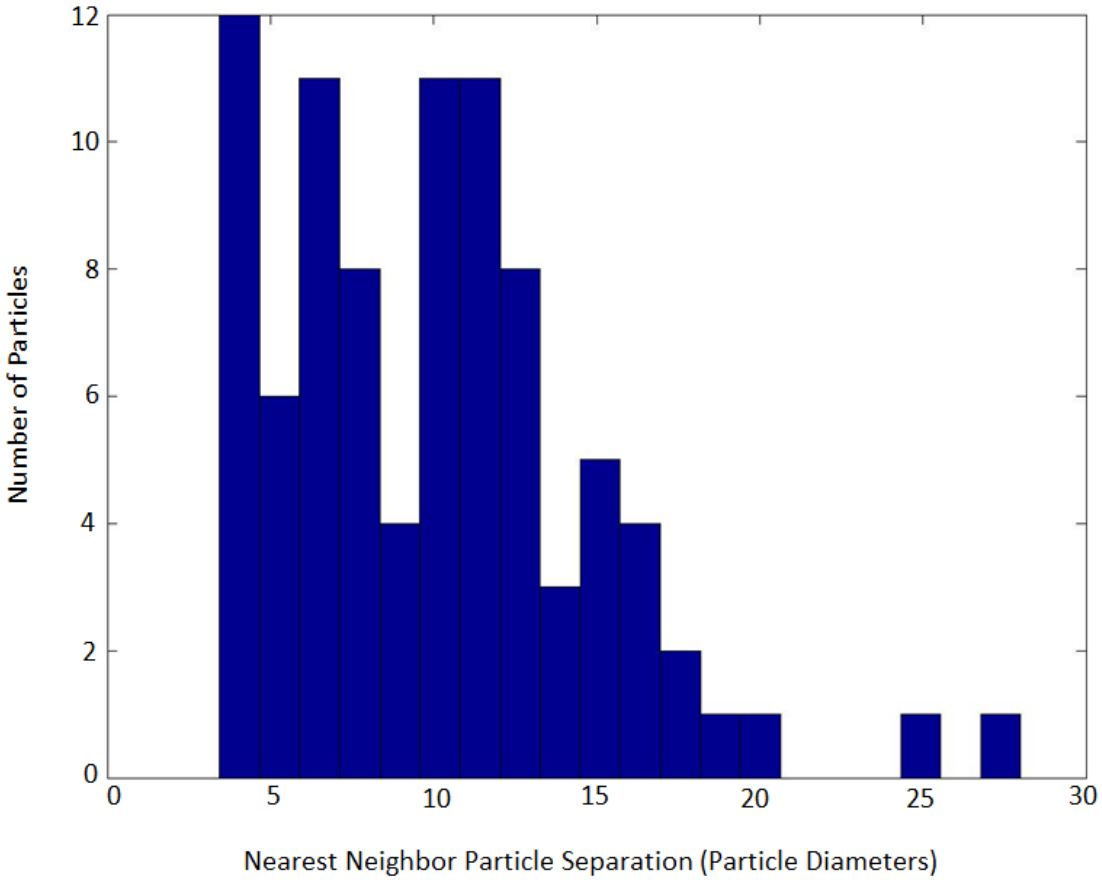

Figure 3.6: Histogram of the nearest neighbor distance for each particle in a single particle removal test

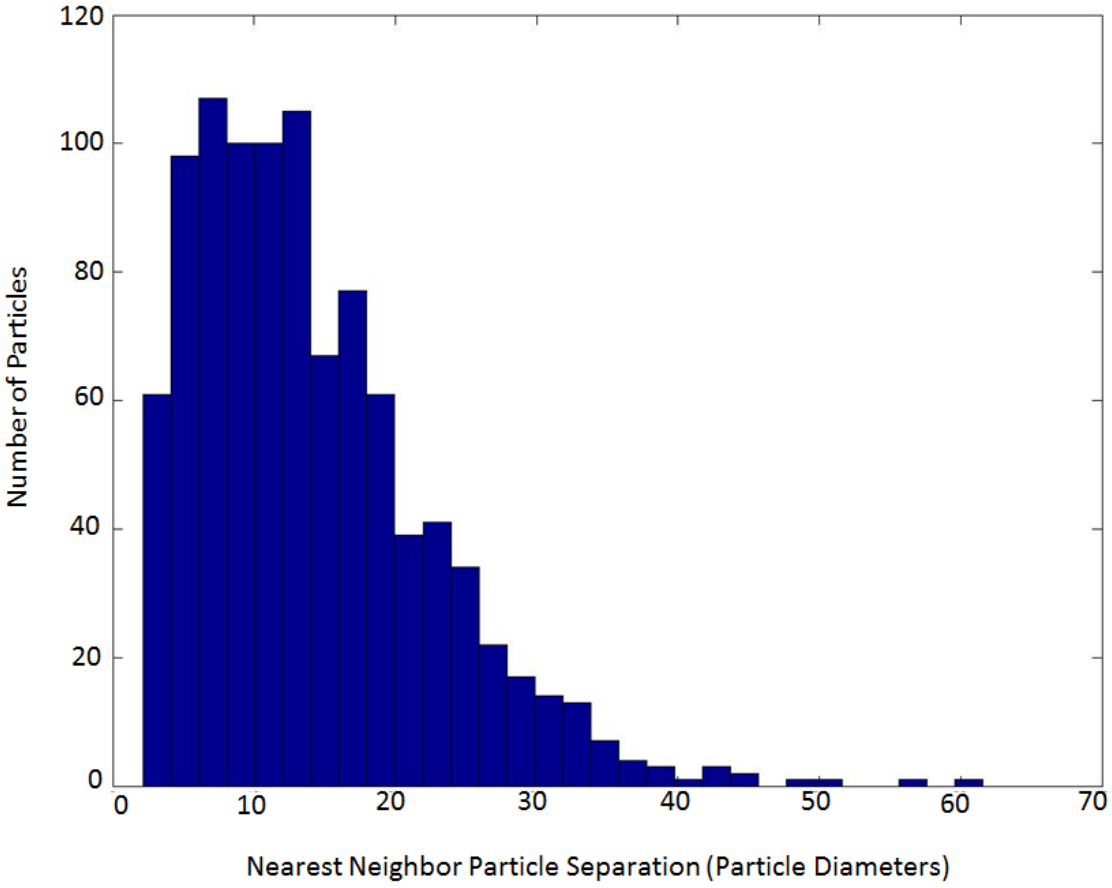

Figure 3.7: Histogram of the nearest neighbor distance for each particle in an entire data set for r = 75 mm and H = 150 mm

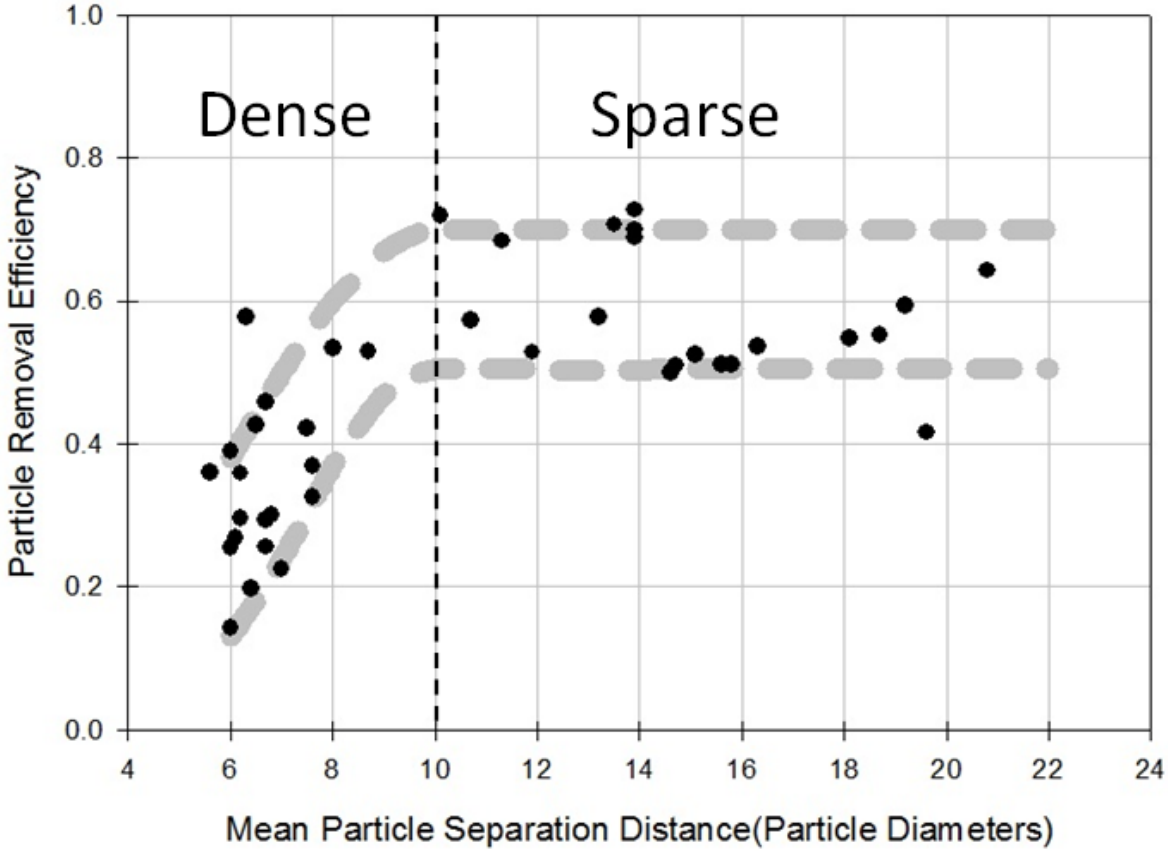

Figure 3.8: Removal efficiency vs. mean particle separation for r = 75 mm and H = 150mm (r/H = 0.5). For a separation greater than 10 particle diameters, removal efficiency becomes independent of particle separation distance

a function of normalized radius r/H from the jet impingement point for sparse particle distributions.

Figure 3.9 reveals that the maximum particle removal efficiency occurs around r/H = 0.1. This location is near the location of maximum shear stress according to the OFI results shown earlier. The error bars shown in r/H are due to the 6-mm width of the viewing field, while the error in removal efficiency is represented as one standard deviation of each data set. The data in Figure 3.9 consist of twenty repeated experiments performed at r/H values of 0.2 and 0.5, and ten repeats performed at all other radial distances. The standard deviation and mean removal efficiency were not affected when 10 additional tests were performed beyond the initial 10 at r/H = 0.2 and 0.5. Therefore it was concluded that ten tests at each radial location were sufficient for meaningful statistics.

Using the experimental OFI data from Figure 2.7, the aerodynamic shear stress at each r/H location tested in Figure 3.9 can be determined from the known jet standoff distance, radial distance from the impingement point, jet exit velocity, and nozzle diameter. This was done using subsonic-jet-exit data only, and the results were combined with those of Figure 3.9 to produce Figure 3.10, which shows particle removal efficiency as a function of the non-dimensional shear stress applied by the impinging jet.
The error bars in shear stress in Figure 3.9 are derived from the experimental results of Figure 2.7. The width of the field-of-view in the particle removal experiments is 6 mm, which corresponds to an error in r/H of ±0.02 for a jet standoff distance of 150 mm. The shear stress varies with r/H, and because r/H varies in each particle removal test due to the width of the field-of-view, the shear stress also varies from one side of the field-of-

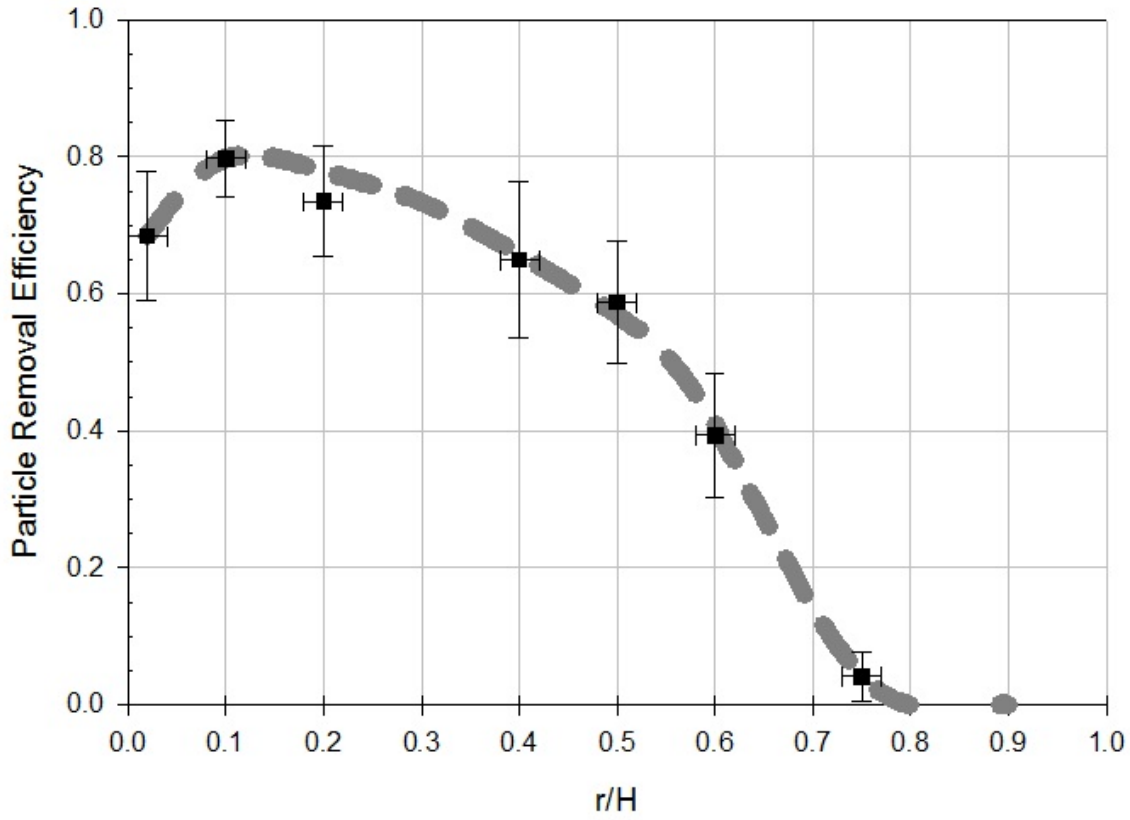

Figure 3.9: Sparse-distribution particle removal efficiency for various radial distances from the jet impingement point at a nozzle standoff distance of 150 mm. The jet pressure ratio was $P_{jet}/P_{atm} = 1.11$, with a jet duration of 0.02 s. Vertical error bars represent the standard deviation of the mean. Horizontal error bars correspond to the 6mm width of the viewing field.

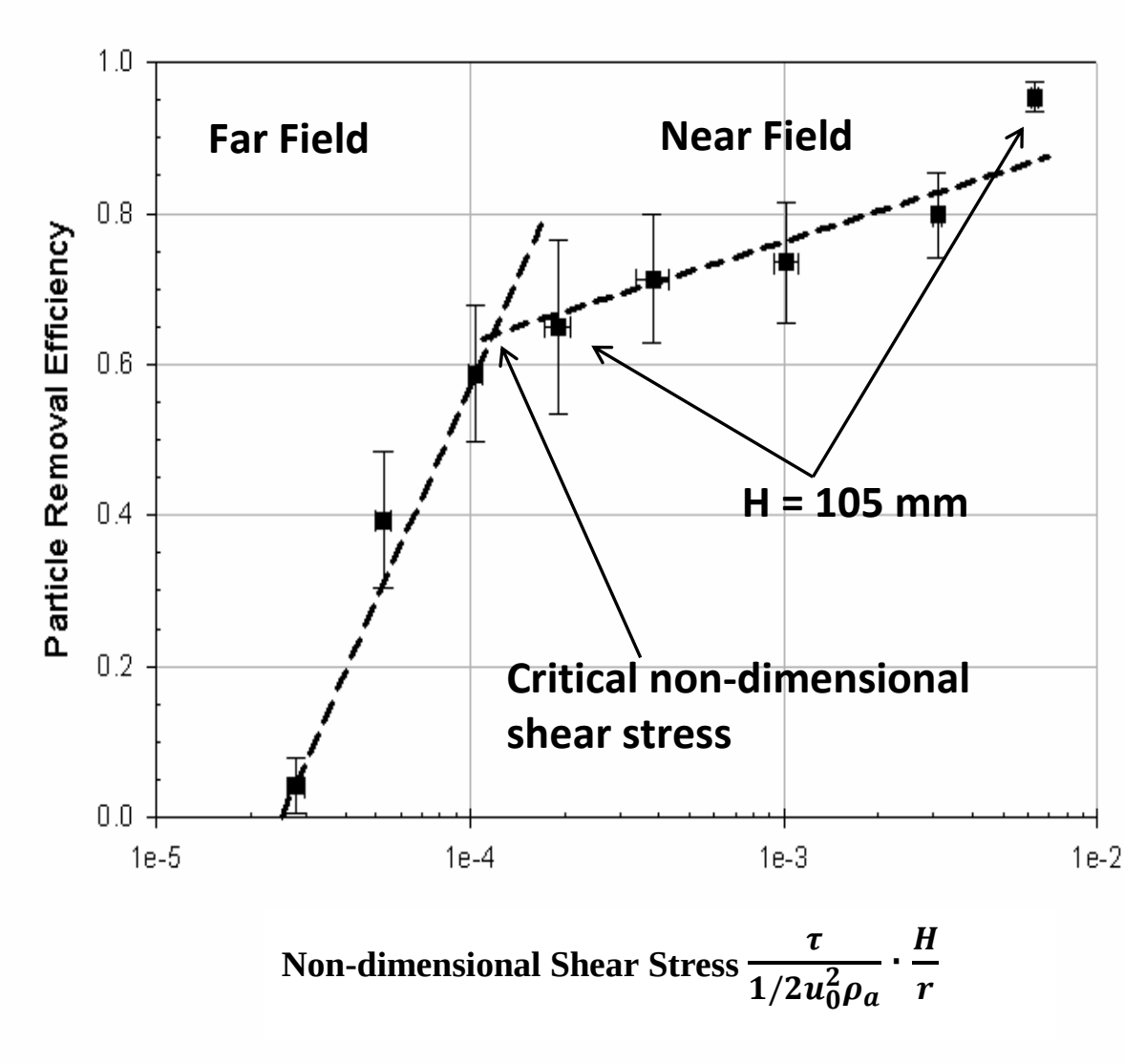

Figure 3.10: Particle removal efficiency vs. nondimensionalized shear stress. Data were taken for a sparse distribution (mean particle separation greater than 10 particle diameters). Vertical error bars represent the standard deviation of the average removal efficiency and horizontal error bars represent the change in shear stress based on the 6mm width of the viewing field.

view to the other. Thus the range of shear stress for each r/H location yields the corresponding error bar shown in Figure 3.10. Additional data were taken at a nozzle standoff distance of 105 mm, and are included in Figure 3.10 where indicated. The removal efficiency is found to follow the same trend as the data of Figure 3.10 having standoff distance of 150 mm.

The results of Figure 3.10 show a sharp change in the trend of particle removal efficiency at a non-dimensionalized wall shear stress value of about 10^{-4}. Below this value – in the far field of the jet-impingement phenomenon – the aerodynamic shear stress is marginal or too low to cause significant removal of the present particles from the substrate. However, above a non-dimensionalized wall shear stress value of about 10^{-4} – in the near field of the jet-impingement phenomenon – Figure 3.10 shows a consistent trend of particle removal efficiency in the 60-90% range. Figure 3.11 shows the near- and far-field regions of the air flow.

For this experiment, then, we can define a critical shear stress level (τ_{cr}) of about 1 Pa, based on the observed non-dimensionalized shear stress value of about 10^{-4}. Using the jet-impingement shear-stress data of Figure 2.6 as an example, the critical value of shear stress for particle removal occurs at a radius of 0.05 – 0.06 m. This is the effective radius of near-field particle removal for the present test conditions, since outside this radius τ is less than τ_{cr}, in the far-field of the jet impingement, so few particles are removed as a result of the jet impingement airflow. For many practical applications of particle resuspension from surfaces by gas-jet impingement, it is important to have such a criterion for the effective radius of the process.

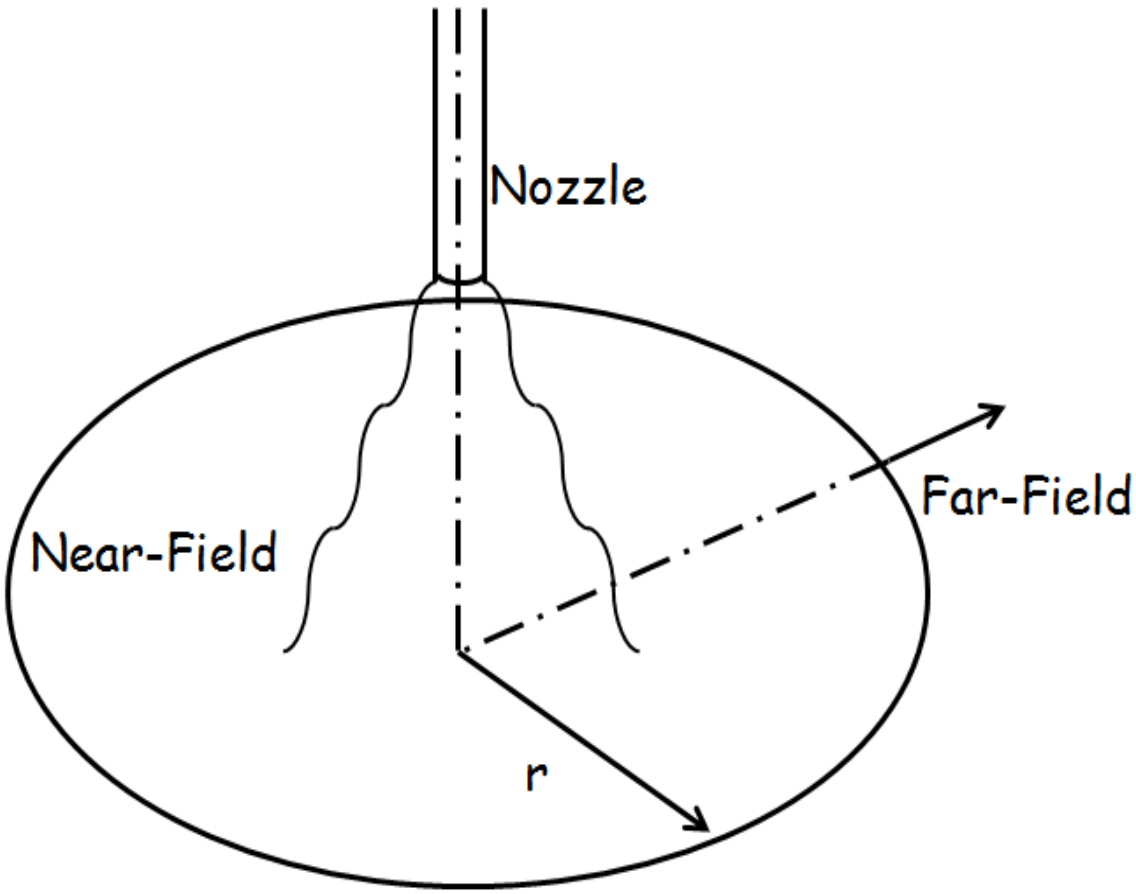

Figure 3.11: Schematic of the near- and far-field regions of air flow. (r represents the effective radius for particle removal, where $\tau = \tau_{cr}$, for sparse distributions)

Chapter 4

CONCLUSIONS

The mean shear stress profile of a round turbulent air jet impinging normally upon a surface has been determined using oil-film interferometry. Experiments were performed for subsonic nozzle exit flows, where $P_{jet}/P_{atm} = 1.11 \pm 0.04$, with jet standoff distances of 0.06 m and 0.075 m, and for sonic exit flows, where $P_{jet}/P_{atm} = 2.52 \pm 0.04$, with jet standoff distances of 0.12 m and 0.165 m. When the resulting data were normalized in terms of r/H (radial distance from the jet impingement point divided by the jet standoff distance) and τ/τ_{max}, all four cases yielded very comparable results. These experiments show that a shear stress maximum occurs at a normalized radial distance from the jet impingement point, r/H, of about 0.09.

These results were compared with those of Smedley, et al. [1], who inferred wall shear stress from particle-removal experiments. The two data sets are similar, but they differ especially at larger values of r/H. This raises questions about particle resuspension by air-jet impingement in dense versus sparse particle distributions.

Further experiments considered the resuspension of 31 μm-diameter latex microspheres from a flat glass substrate using the same impinging round turbulent jet flow that yielded the shear stress results. Widely-differing particle densities on the glass substrate were tested at one jet impingement condition. This revealed that the particle removal efficiency of the impinging jet flow can only be considered independent of particle distribution density when the mean distance between particles is at least 10 particle diameters. We refer to such a condition as a "sparse" particle distribution. Until

now, there has been no such definition in the literature of sparse versus dense particle distributions. Only sparse particle distributions were used in the remainder of the study.

Further experiments then measured the particle removal efficiency as a function of local mean shear stress produced by the impinging-jet flowfield, measured earlier in this study. This revealed that there is a threshold value of non-dimensionalized shear stress, approximately 10^{-4}, below which few particles are removed from the substrate. For given jet conditions, a corresponding critical shear stress (τ_{cr}) can be derived, which for our experiments is about 1 Pa. Where τ is greater than τ_{cr}, consistent particle removal efficiencies in the 60-95% range are observed. We conclude that τ_{cr} can be used to define the effective radius of particle removal due to round turbulent air jet impingement on a planar surface.

APPENDIX A: Particle Counting MATLAB Code

```
clear all;
close all;


z=1;


cont = 1;
while cont == 1


    cont = input('Do you want to continue? ');
     if cont ~=1
        break
    end



datestring = input('What is the date (yyyymmdd) ');
run_number = input('What run number? ');
last_pic = input('What is the last picture? ');
h = input('What is the jet height? ');
r = input('What is the radial distance from the impingement point? ');
first_pic = 1;


pulse_diam = '02p_31d';


base_folder = 'Z:/rmy5009/Particle Removal/Data';
folder_name = [base_folder, '/h=', num2str(h), '/r=', num2str(r), '/'];
```

```
calibration_pic_filename = [folder_name, num2str(datestring),
'_calibrate/', num2str(datestring), '_calibrate', num2str(1, '%06d'),
'.tif'];


pic_name = [pulse_diam, '_', num2str(datestring), '_',
num2str(run_number)];
before_pic_filename = [folder_name, pic_name, '/', pic_name,
num2str(first_pic, '%06d'), '.tif'];
after_pic_filename = [folder_name, pic_name, '/', pic_name,
num2str(last_pic, '%06d'), '.tif'];


calibration = -double(imadjust(imread(calibration_pic_filename)));
before_pic = -double(imadjust(imread(before_pic_filename)));
after_pic = -double(imadjust(imread(after_pic_filename)));


before_hatted = imsubtract(imadd(before_pic, imtophat(before_pic,
strel('disk', 6))), imbothat(before_pic, strel('disk', 6)));
after_hatted = imsubtract(imadd(after_pic, imtophat(after_pic,
strel('disk', 6))), imbothat(after_pic, strel('disk', 6)));
calib_hatted = imsubtract(imadd(calibration, imtophat(calibration,
strel('disk', 6))), imbothat(calibration, strel('disk', 6)));


before_processed = before_hatted - calib_hatted;
after_processed = after_hatted - calib_hatted;


%figure; imagesc(before_processed);
%figure; imagesc(after_processed);
```

```
%%

before_processed_binary = bwmorph(before_processed > 40, 'majority',
10);
after_processed_binary = bwmorph(after_processed > 40, 'majority', 10);

%figure; imagesc(before_processed .* before_processed_binary);
%figure; imagesc(after_processed .* after_processed_binary);

particle_count_initial = bweuler(before_processed_binary, 8)
particle_count_final = bweuler(after_processed_binary, 8)

particle_count_removed = particle_count_initial - particle_count_final;
particle_removal_efficiency = particle_count_removed /
particle_count_initial

%%

before_processed = before_processed .* before_processed_binary;
after_processed = after_processed .* after_processed_binary;

% before_edges = abs(gradient(before_processed')') +
abs(gradient(before_processed));
% before_edges_removed = before_processed - before_edges; %.*
double(~before_edges);

% before_dilated = imdilate(before_processed, strel('disk', 1));
```

```
% after_dilated = imdilate(after_processed, strel('disk', 1));


particle_pixel_sum = zeros(1, 10);
for k = 0:9
    se = strel('disk', k);
    fo = imopen(before_processed, se);
    particle_pixel_sum(k+1) = sum(fo(:));
end


%% Nearest Neighbor


morph = bwmorph(before_processed_binary, 'shrink', inf);
count = 1;
dist = 0;
% [nn,L] = bwdist(morph);


morph_counted = uint16(morph);


for i=1: size(morph,1)
    for j=1:size(morph,2)
        if morph(i,j)==1
            particle_x(count) = i;
            particle_y(count) = j;


            morph_counted(i,j) = count;
            count = count + 1;
        end
    end
```

```
end

num_particles = length(particle_x);
distance_matrix = zeros(num_particles, num_particles);

for i=1:size(distance_matrix,1)
    for j=1:size(distance_matrix,2)
        distance_matrix(i,j) = sqrt((particle_x(i) - particle_x(j))^2 +
(particle_y(i) - particle_y(j))^2);
    end
end

distance_matrix_modified = distance_matrix;
for i=1:num_particles
    distance_matrix_modified(i,i) = 1e6;
    nearest_neighbor(i) = min(distance_matrix_modified(:,i));
end

mean_particle_separation = mean(nearest_neighbor)*.1767/15/.031

average_total_distance =
sum(sum(distance_matrix))*.1767/15/.031/(num_particles^2-num_particles)

%% Average Distance
%x = 0:(num_particles - 1);
%for i=1:num_particles

%particle = distance_matrix(1:num_particles,i);
```

```
%part_order = sort(particle);


%for i=1:num_particles
   % average_dist_pix(i) = mean(part_order(1:i,1));
%end


%average_distance_plot = average_dist_pix.*.1767/15;


%plot(x,average_distance_plot)
%xlabel('Number of Particles')
%ylabel('Average Particle Distance (mm)')
%hold on
%end


%% Nearest Neighbor Histogram


nearest_neighbor_mm = nearest_neighbor*.1767/15/.031;
name = genvarname(['nearest_neighbor_mm' num2str(z)]);
name = nearest_neighbor_mm;
save(['nn' num2str(z)],'name')
nbins = 30;
figure, hist(nearest_neighbor_mm, nbins);
title('Histogram of Distance to Nearest Neighbor');


z = 1+z;


end
```

APPENDIX B: Subsonic Nozzle-Exit Data

Table B.1: Run 1; Jet Height = 7 .5 cm; Test duration = 50 s

Radius (m)	Spacing(m)	Fringe Number (N)	Height(m)	Tau(Pa)	R/H
0.000E+00			0.000E+00		0.000E+00
4.251E-03	4.251E-03	2.000E+00	2.676E-07	1.647E+00	5.668E-02
7.627E-03	3.377E-03	3.000E+00	4.014E-07	2.338E+00	1.017E-01
1.013E-02	2.502E-03	4.000E+00	5.352E-07	2.340E+00	1.351E-01
1.218E-02	2.050E-03	5.000E+00	6.690E-07	2.213E+00	1.624E-01
1.351E-02	1.326E-03	6.000E+00	8.028E-07	1.931E+00	1.801E-01
1.489E-02	1.387E-03	7.000E+00	9.366E-07	1.775E+00	1.986E-01
1.610E-02	1.206E-03	8.000E+00	1.070E-06	1.635E+00	2.147E-01
1.737E-02	1.266E-03	9.000E+00	1.204E-06	1.556E+00	2.315E-01
1.833E-02	9.647E-04	1.000E+01	1.338E-06	1.446E+00	2.444E-01
1.911E-02	7.838E-04	1.100E+01	1.472E-06	1.333E+00	2.548E-01
2.011E-02	9.949E-04	1.200E+01	1.606E-06	1.282E+00	2.681E-01
2.098E-02	8.743E-04	1.300E+01	1.739E-06	1.228E+00	2.798E-01

Table B.2: Run 2; Jet Height = 7 .5 cm; Test duration = 40 s

Radius (m)	Spacing(m)	Fringe Number (N)	Height(m)	Tau(Pa)	R/H
2.412E-03			0.000E+00		3.216E-02
3.949E-03	1.538E-03	1.000E+00	1.338E-07	1.144E+01	5.266E-02
6.241E-03	2.291E-03	2.000E+00	2.676E-07	1.423E+01	8.321E-02
8.230E-03	1.990E-03	3.000E+00	4.014E-07	1.380E+01	1.097E-01
9.828E-03	1.598E-03	4.000E+00	5.352E-07	1.244E+01	1.310E-01
1.131E-02	1.477E-03	5.000E+00	6.690E-07	1.148E+01	1.507E-01
1.269E-02	1.387E-03	6.000E+00	8.028E-07	1.079E+01	1.692E-01
1.378E-02	1.085E-03	7.000E+00	9.366E-07	9.844E+00	1.837E-01
1.483E-02	1.055E-03	8.000E+00	1.070E-06	9.173E+00	1.978E-01
1.586E-02	1.025E-03	9.000E+00	1.204E-06	8.679E+00	2.114E-01
1.676E-02	9.044E-04	1.000E+01	1.338E-06	8.181E+00	2.235E-01
1.761E-02	8.441E-04	1.100E+01	1.472E-06	7.746E+00	2.348E-01
1.833E-02	7.235E-04	1.200E+01	1.606E-06	7.286E+00	2.444E-01
1.905E-02	7.235E-04	1.300E+01	1.739E-06	6.927E+00	2.540E-01
1.987E-02	8.140E-04	1.400E+01	1.873E-06	6.734E+00	2.649E-01

Table B.3: Run 2; Jet Height = 7 .5 cm; Test duration = 50 s

Radius (m)	Spacing(m)	Fringe Number (N)	Height(m)	Tau(Pa)	R/H
2.412E-03			0.000E+00		3.216E-02
4.522E-03	2.110E-03	1.000E+00	1.338E-07	1.225E+01	6.030E-02
7.235E-03	2.713E-03	2.000E+00	2.676E-07	1.374E+01	9.647E-02
9.376E-03	2.140E-03	3.000E+00	4.014E-07	1.241E+01	1.250E-01
1.143E-02	2.050E-03	4.000E+00	5.352E-07	1.179E+01	1.523E-01
1.293E-02	1.507E-03	5.000E+00	6.690E-07	1.047E+01	1.724E-01
1.423E-02	1.296E-03	6.000E+00	8.028E-07	9.373E+00	1.897E-01
1.553E-02	1.296E-03	7.000E+00	9.366E-07	8.711E+00	2.070E-01
1.667E-02	1.146E-03	8.000E+00	1.070E-06	8.102E+00	2.223E-01
1.773E-02	1.055E-03	9.000E+00	1.204E-06	7.589E+00	2.364E-01
1.878E-02	1.055E-03	1.000E+01	1.338E-06	7.232E+00	2.504E-01
1.960E-02	8.140E-04	1.100E+01	1.472E-06	6.744E+00	2.613E-01
2.047E-02	8.743E-04	1.200E+01	1.606E-06	6.426E+00	2.729E-01
2.116E-02	6.934E-04	1.300E+01	1.739E-06	6.034E+00	2.822E-01
2.189E-02	7.235E-04	1.400E+01	1.873E-06	5.743E+00	2.918E-01
2.264E-02	7.537E-04	1.500E+01	2.007E-06	5.532E+00	3.019E-01
2.339E-02	7.537E-04	1.600E+01	2.141E-06	5.365E+00	3.119E-01

Table B.4: Run 2; Jet Height = 7 .5 cm; Test duration = 60 s

Radius (m)	Spacing(m)	Fringe Number (N)	Height(m)	Tau(Pa)	R/H
2.412E-03			0.000E+00		3.216E-02
5.125E-03	2.713E-03	1.000E+00	1.338E-07	1.295E+01	6.833E-02
8.170E-03	3.045E-03	2.000E+00	2.676E-07	1.337E+01	1.089E-01
1.064E-02	2.472E-03	3.000E+00	4.014E-07	1.206E+01	1.419E-01
1.281E-02	2.171E-03	4.000E+00	5.352E-07	1.105E+01	1.708E-01
1.432E-02	1.507E-03	5.000E+00	6.690E-07	9.491E+00	1.909E-01
1.583E-02	1.507E-03	6.000E+00	8.028E-07	8.624E+00	2.110E-01
1.709E-02	1.266E-03	7.000E+00	9.366E-07	7.820E+00	2.279E-01
1.839E-02	1.296E-03	8.000E+00	1.070E-06	7.339E+00	2.452E-01
1.942E-02	1.025E-03	9.000E+00	1.204E-06	6.762E+00	2.589E-01
2.053E-02	1.115E-03	1.000E+01	1.338E-06	6.433E+00	2.737E-01
2.147E-02	9.346E-04	1.100E+01	1.472E-06	6.056E+00	2.862E-01
2.228E-02	8.140E-04	1.200E+01	1.606E-06	5.682E+00	2.971E-01
2.318E-02	9.044E-04	1.300E+01	1.739E-06	5.456E+00	3.091E-01
2.391E-02	7.235E-04	1.400E+01	1.873E-06	5.165E+00	3.188E-01
2.457E-02	6.632E-04	1.500E+01	2.007E-06	4.893E+00	3.276E-01
2.517E-02	6.030E-04	1.600E+01	2.141E-06	4.636E+00	3.356E-01

Table B.5: Run 2; Jet Height = 7 .5 cm; Test duration = 70 s

Radius (m)	Spacing(m)	Fringe Number (N)	Height(m)	Tau(Pa)	R/H
2.412E-03			0.000E+00		3.216E-02
5.457E-03	3.045E-03	1.000E+00	1.338E-07	1.363E+01	7.276E-02
9.135E-03	3.678E-03	2.000E+00	2.676E-07	1.380E+01	1.218E-01
1.170E-02	2.563E-03	3.000E+00	4.014E-07	1.144E+01	1.560E-01
1.375E-02	2.050E-03	4.000E+00	5.352E-07	9.791E+00	1.833E-01
1.556E-02	1.809E-03	5.000E+00	6.690E-07	8.732E+00	2.074E-01
1.712E-02	1.568E-03	6.000E+00	8.028E-07	7.898E+00	2.283E-01
1.854E-02	1.417E-03	7.000E+00	9.366E-07	7.253E+00	2.472E-01
1.978E-02	1.236E-03	8.000E+00	1.070E-06	6.674E+00	2.637E-01
2.095E-02	1.176E-03	9.000E+00	1.204E-06	6.230E+00	2.794E-01
2.204E-02	1.085E-03	1.000E+01	1.338E-06	5.851E+00	2.938E-01
2.294E-02	9.044E-04	1.100E+01	1.472E-06	5.448E+00	3.059E-01
2.382E-02	8.743E-04	1.200E+01	1.606E-06	5.123E+00	3.176E-01
2.475E-02	9.346E-04	1.300E+01	1.739E-06	4.911E+00	3.300E-01
2.538E-02	6.331E-04	1.400E+01	1.873E-06	4.580E+00	3.385E-01

Table B.6: Run 2; Jet Height = 7 .5 cm; Test duration = 80 s

Radius (m)	Spacing(m)	Fringe Number (N)	Height(m)	Tau(Pa)	R/H
2.412E-03			0.000E+00		3.216E-02
6.180E-03	3.768E-03	1.000E+00	1.338E-07	1.387E+01	8.240E-02
9.647E-03	3.467E-03	2.000E+00	2.676E-07	1.221E+01	1.286E-01
1.248E-02	2.834E-03	3.000E+00	4.014E-07	1.060E+01	1.664E-01
1.483E-02	2.352E-03	4.000E+00	5.352E-07	9.346E+00	1.978E-01
1.676E-02	1.929E-03	5.000E+00	6.690E-07	8.283E+00	2.235E-01
1.839E-02	1.628E-03	6.000E+00	8.028E-07	7.409E+00	2.452E-01
1.981E-02	1.417E-03	7.000E+00	9.366E-07	6.700E+00	2.641E-01
2.131E-02	1.507E-03	8.000E+00	1.070E-06	6.331E+00	2.842E-01
2.222E-02	9.044E-04	9.000E+00	1.204E-06	5.649E+00	2.963E-01
2.355E-02	1.326E-03	1.000E+01	1.338E-06	5.439E+00	3.139E-01
2.442E-02	8.743E-04	1.100E+01	1.472E-06	5.021E+00	3.256E-01
2.520E-02	7.838E-04	1.200E+01	1.606E-06	4.649E+00	3.360E-01
2.620E-02	9.949E-04	1.300E+01	1.739E-06	4.469E+00	3.493E-01
2.695E-02	7.537E-04	1.400E+01	1.873E-06	4.215E+00	3.594E-01

Table B.7: Run 3; Jet Height = 7 .5 cm; Test duration = 50 s

Radius (m)	Spacing(m)	Fringe Number (N)	Height(m)	Tau(Pa)	R/H
1.963E-03			0.000E+00		2.618E-02
3.805E-03	1.842E-03	1.000E+00	1.338E-07	1.182E+01	5.074E-02
6.524E-03	2.718E-03	2.000E+00	2.676E-07	1.400E+01	8.698E-02
9.000E-03	2.477E-03	3.000E+00	4.014E-07	1.330E+01	1.200E-01
1.084E-02	1.842E-03	4.000E+00	5.352E-07	1.159E+01	1.446E-01
1.253E-02	1.691E-03	5.000E+00	6.690E-07	1.054E+01	1.671E-01
1.401E-02	1.480E-03	6.000E+00	8.028E-07	9.683E+00	1.869E-01
1.525E-02	1.238E-03	7.000E+00	9.366E-07	8.849E+00	2.034E-01
1.646E-02	1.208E-03	8.000E+00	1.070E-06	8.282E+00	2.195E-01
1.740E-02	9.363E-04	9.000E+00	1.204E-06	7.592E+00	2.320E-01
1.839E-02	9.967E-04	1.000E+01	1.338E-06	7.158E+00	2.452E-01
1.930E-02	9.061E-04	1.100E+01	1.472E-06	6.759E+00	2.573E-01
2.021E-02	9.061E-04	1.200E+01	1.606E-06	6.462E+00	2.694E-01
2.087E-02	6.645E-04	1.300E+01	1.739E-06	6.040E+00	2.783E-01
2.159E-02	7.249E-04	1.400E+01	1.873E-06	5.750E+00	2.879E-01

Table B.8: Run 3; Jet Height = 7 .5 cm; Test duration = 60 s

Radius (m)	Spacing(m)	Fringe Number (N)	Height(m)	Tau(Pa)	R/H
1.963E-03			0.000E+00		2.618E-02
4.168E-03	2.205E-03	1.000E+00	1.338E-07	1.168E+01	5.557E-02
7.490E-03	3.322E-03	2.000E+00	2.676E-07	1.392E+01	9.987E-02
1.012E-02	2.628E-03	3.000E+00	4.014E-07	1.238E+01	1.349E-01
1.211E-02	1.993E-03	4.000E+00	5.352E-07	1.067E+01	1.615E-01
1.392E-02	1.812E-03	5.000E+00	6.690E-07	9.641E+00	1.856E-01
1.546E-02	1.540E-03	6.000E+00	8.028E-07	8.762E+00	2.062E-01
1.679E-02	1.329E-03	7.000E+00	9.366E-07	7.998E+00	2.239E-01
1.800E-02	1.208E-03	8.000E+00	1.070E-06	7.381E+00	2.400E-01
1.912E-02	1.117E-03	9.000E+00	1.204E-06	6.877E+00	2.549E-01
2.014E-02	1.027E-03	1.000E+01	1.338E-06	6.444E+00	2.686E-01
2.117E-02	1.027E-03	1.100E+01	1.472E-06	6.131E+00	2.823E-01
2.187E-02	6.947E-04	1.200E+01	1.606E-06	5.654E+00	2.916E-01
2.274E-02	8.759E-04	1.300E+01	1.739E-06	5.404E+00	3.032E-01

Table B.9: Run 3; Jet Height = 7 .5 cm; Test duration = 70 s

Radius (m)	Spacing(m)	Fringe Number (N)	Height(m)	Tau(Pa)	R/H
1.963E-03			0.000E+00		2.618E-02
4.863E-03	2.899E-03	1.000E+00	1.338E-07	1.267E+01	6.483E-02
8.275E-03	3.413E-03	2.000E+00	2.676E-07	1.272E+01	1.103E-01
1.121E-02	2.930E-03	3.000E+00	4.014E-07	1.165E+01	1.494E-01
1.323E-02	2.024E-03	4.000E+00	5.352E-07	9.817E+00	1.764E-01
1.513E-02	1.903E-03	5.000E+00	6.690E-07	8.813E+00	2.018E-01
1.691E-02	1.782E-03	6.000E+00	8.028E-07	8.181E+00	2.255E-01
1.818E-02	1.268E-03	7.000E+00	9.366E-07	7.296E+00	2.424E-01
1.948E-02	1.299E-03	8.000E+00	1.070E-06	6.749E+00	2.597E-01
2.060E-02	1.117E-03	9.000E+00	1.204E-06	6.234E+00	2.746E-01
2.172E-02	1.117E-03	1.000E+01	1.338E-06	5.872E+00	2.895E-01
2.256E-02	8.457E-04	1.100E+01	1.472E-06	5.423E+00	3.008E-01
2.356E-02	9.967E-04	1.200E+01	1.606E-06	5.177E+00	3.141E-01
2.431E-02	7.551E-04	1.300E+01	1.739E-06	4.850E+00	3.242E-01

Table B.10: Run 4; Jet Height = 7 .5 cm; Test duration = 50 s

Radius (m)	Spacing(m)	Fringe Number (N)	Height(m)	Tau(Pa)	R/H
1.873E-03			0.000E+00		2.497E-02
3.624E-03	1.752E-03	1.000E+00	1.338E-07	1.145E+01	4.832E-02
6.101E-03	2.477E-03	2.000E+00	2.676E-07	1.295E+01	8.135E-02
8.638E-03	2.537E-03	3.000E+00	4.014E-07	1.293E+01	1.152E-01
1.054E-02	1.903E-03	4.000E+00	5.352E-07	1.150E+01	1.405E-01
1.217E-02	1.631E-03	5.000E+00	6.690E-07	1.036E+01	1.623E-01
1.365E-02	1.480E-03	6.000E+00	8.028E-07	9.549E+00	1.820E-01
1.492E-02	1.268E-03	7.000E+00	9.366E-07	8.789E+00	1.989E-01
1.598E-02	1.057E-03	8.000E+00	1.070E-06	8.036E+00	2.130E-01
1.706E-02	1.087E-03	9.000E+00	1.204E-06	7.555E+00	2.275E-01
1.809E-02	1.027E-03	1.000E+01	1.338E-06	7.159E+00	2.412E-01
1.900E-02	9.061E-04	1.100E+01	1.472E-06	6.760E+00	2.533E-01
1.981E-02	8.155E-04	1.200E+01	1.606E-06	6.380E+00	2.642E-01
2.060E-02	7.853E-04	1.300E+01	1.739E-06	6.062E+00	2.746E-01

Table B.11: Run 4; Jet Height = 7 .5 cm; Test duration = 60 s

Radius (m)	Spacing(m)	Fringe Number (N)	Height(m)	Tau(Pa)	R/H
1.873E-03			0.000E+00		2.497E-02
4.077E-03	2.205E-03	1.000E+00	1.338E-07	1.182E+01	5.436E-02
7.128E-03	3.050E-03	2.000E+00	2.676E-07	1.303E+01	9.504E-02
9.846E-03	2.718E-03	3.000E+00	4.014E-07	1.215E+01	1.313E-01
1.187E-02	2.024E-03	4.000E+00	5.352E-07	1.060E+01	1.583E-01
1.362E-02	1.752E-03	5.000E+00	6.690E-07	9.511E+00	1.816E-01
1.504E-02	1.420E-03	6.000E+00	8.028E-07	8.500E+00	2.005E-01
1.640E-02	1.359E-03	7.000E+00	9.366E-07	7.832E+00	2.187E-01
1.764E-02	1.238E-03	8.000E+00	1.070E-06	7.286E+00	2.352E-01
1.873E-02	1.087E-03	9.000E+00	1.204E-06	6.775E+00	2.497E-01
1.975E-02	1.027E-03	1.000E+01	1.338E-06	6.359E+00	2.634E-01
2.078E-02	1.027E-03	1.100E+01	1.472E-06	6.056E+00	2.771E-01
2.159E-02	8.155E-04	1.200E+01	1.606E-06	5.676E+00	2.879E-01
2.250E-02	9.061E-04	1.300E+01	1.739E-06	5.442E+00	3.000E-01
2.323E-02	7.249E-04	1.400E+01	1.873E-06	5.145E+00	3.097E-01

Table B.12: Run 5; Jet Height = 7 .5 cm; Test duration = 50 s

Radius (m)	Spacing(m)	Fringe Number (N)	Height(m)	Tau(Pa)	R/H
3.062E-03			0.000E+00		4.083E-02
5.025E-03	1.963E-03	1.000E+00	1.338E-07	1.266E+01	6.700E-02
7.621E-03	2.597E-03	2.000E+00	2.676E-07	1.426E+01	1.016E-01
9.644E-03	2.023E-03	3.000E+00	4.014E-07	1.243E+01	1.286E-01
1.152E-02	1.872E-03	4.000E+00	5.352E-07	1.136E+01	1.536E-01
1.297E-02	1.449E-03	5.000E+00	6.690E-07	1.005E+01	1.729E-01
1.438E-02	1.419E-03	6.000E+00	8.028E-07	9.293E+00	1.918E-01
1.562E-02	1.238E-03	7.000E+00	9.366E-07	8.599E+00	2.083E-01
1.674E-02	1.117E-03	8.000E+00	1.070E-06	8.003E+00	2.232E-01
1.768E-02	9.360E-04	9.000E+00	1.204E-06	7.386E+00	2.357E-01
1.873E-02	1.057E-03	1.000E+01	1.338E-06	7.073E+00	2.498E-01
1.955E-02	8.152E-04	1.100E+01	1.472E-06	6.616E+00	2.606E-01
2.042E-02	8.756E-04	1.200E+01	1.606E-06	6.322E+00	2.723E-01
2.118E-02	7.548E-04	1.300E+01	1.739E-06	5.997E+00	2.824E-01
2.193E-02	7.548E-04	1.400E+01	1.873E-06	5.740E+00	2.924E-01
2.263E-02	6.944E-04	1.500E+01	2.007E-06	5.492E+00	3.017E-01

Table B.13: Run 5; Jet Height = 7 .5 cm; Test duration = 60 s

Radius (m)	Spacing(m)	Fringe Number (N)	Height(m)	Tau(Pa)	R/H
3.062E-03			0.000E+00		4.083E-02
5.538E-03	2.476E-03	1.000E+00	1.338E-07	1.286E+01	7.384E-02
8.316E-03	2.778E-03	2.000E+00	2.676E-07	1.294E+01	1.109E-01
1.073E-02	2.415E-03	3.000E+00	4.014E-07	1.178E+01	1.431E-01
1.272E-02	1.993E-03	4.000E+00	5.352E-07	1.049E+01	1.697E-01
1.451E-02	1.781E-03	5.000E+00	6.690E-07	9.559E+00	1.934E-01
1.595E-02	1.449E-03	6.000E+00	8.028E-07	8.620E+00	2.127E-01
1.713E-02	1.178E-03	7.000E+00	9.366E-07	7.728E+00	2.284E-01
1.834E-02	1.208E-03	8.000E+00	1.070E-06	7.183E+00	2.445E-01
1.949E-02	1.147E-03	9.000E+00	1.204E-06	6.767E+00	2.598E-01
2.048E-02	9.964E-04	1.000E+01	1.338E-06	6.348E+00	2.731E-01
2.136E-02	8.756E-04	1.100E+01	1.472E-06	5.943E+00	2.848E-01
2.220E-02	8.454E-04	1.200E+01	1.606E-06	5.612E+00	2.961E-01
2.299E-02	7.850E-04	1.300E+01	1.739E-06	5.313E+00	3.065E-01
2.377E-02	7.850E-04	1.400E+01	1.873E-06	5.076E+00	3.170E-01
2.465E-02	8.756E-04	1.500E+01	2.007E-06	4.940E+00	3.287E-01

Table B.14: Run 6; Jet Height = 7 .5 cm; Test duration = 90 s

Radius (m)	Spacing(m)	Fringe Number (N)	Height(m)	Tau(Pa)	R/H
1.710E-02			0.000E+00		2.280E-01
1.876E-02	1.656E-03	1.000E+00	1.338E-07	6.683E+00	2.501E-01
2.033E-02	1.566E-03	2.000E+00	2.676E-07	6.167E+00	2.710E-01
2.177E-02	1.445E-03	3.000E+00	4.014E-07	5.697E+00	2.903E-01
2.307E-02	1.295E-03	4.000E+00	5.352E-07	5.243E+00	3.075E-01
2.430E-02	1.235E-03	5.000E+00	6.690E-07	4.940E+00	3.240E-01
2.538E-02	1.084E-03	6.000E+00	8.028E-07	4.606E+00	3.385E-01
2.635E-02	9.636E-04	7.000E+00	9.366E-07	4.283E+00	3.513E-01
2.728E-02	9.335E-04	8.000E+00	1.070E-06	4.042E+00	3.637E-01
2.812E-02	8.431E-04	9.000E+00	1.204E-06	3.807E+00	3.750E-01
2.891E-02	7.829E-04	1.000E+01	1.338E-06	3.595E+00	3.854E-01
2.969E-02	7.829E-04	1.100E+01	1.472E-06	3.436E+00	3.959E-01
3.044E-02	7.528E-04	1.200E+01	1.606E-06	3.298E+00	4.059E-01
3.117E-02	7.227E-04	1.300E+01	1.739E-06	3.174E+00	4.155E-01
3.183E-02	6.625E-04	1.400E+01	1.873E-06	3.048E+00	4.244E-01
3.246E-02	6.323E-04	1.500E+01	2.007E-06	2.932E+00	4.328E-01
3.303E-02	5.721E-04	1.600E+01	2.141E-06	2.811E+00	4.404E-01

Table B.15: Run 6; Jet Height = 7 .5 cm; Test duration = 100 s

Radius (m)	Spacing(m)	Fringe Number (N)	Height(m)	Tau(Pa)	R/H
1.710E-02			0.000E+00		2.280E-01
1.897E-02	1.867E-03	1.000E+00	1.338E-07	6.572E+00	2.529E-01
2.072E-02	1.746E-03	2.000E+00	2.676E-07	6.088E+00	2.762E-01
2.225E-02	1.536E-03	3.000E+00	4.014E-07	5.527E+00	2.967E-01
2.364E-02	1.385E-03	4.000E+00	5.352E-07	5.077E+00	3.152E-01
2.487E-02	1.235E-03	5.000E+00	6.690E-07	4.673E+00	3.316E-01
2.605E-02	1.174E-03	6.000E+00	8.028E-07	4.385E+00	3.473E-01
2.701E-02	9.636E-04	7.000E+00	9.366E-07	4.024E+00	3.601E-01
2.806E-02	1.054E-03	8.000E+00	1.070E-06	3.849E+00	3.742E-01
2.897E-02	9.033E-04	9.000E+00	1.204E-06	3.630E+00	3.862E-01
2.984E-02	8.732E-04	1.000E+01	1.338E-06	3.451E+00	3.979E-01
3.071E-02	8.732E-04	1.100E+01	1.472E-06	3.319E+00	4.095E-01
3.144E-02	7.227E-04	1.200E+01	1.606E-06	3.143E+00	4.192E-01
3.213E-02	6.926E-04	1.300E+01	1.739E-06	2.990E+00	4.284E-01
3.285E-02	7.227E-04	1.400E+01	1.873E-06	2.881E+00	4.380E-01
3.357E-02	7.227E-04	1.500E+01	2.007E-06	2.793E+00	4.477E-01
3.412E-02	5.420E-04	1.600E+01	2.141E-06	2.655E+00	4.549E-01
3.466E-02	5.420E-04	1.700E+01	2.275E-06	2.539E+00	4.621E-01
3.526E-02	6.022E-04	1.800E+01	2.408E-06	2.462E+00	4.701E-01

Table B.16: Run 6; Jet Height = 7 .5 cm; Test duration = 110 s

Radius (m)	Spacing(m)	Fringe Number (N)	Height(m)	Tau(Pa)	R/H
1.710E-02			0.000E+00		2.280E-01
1.921E-02	2.108E-03	1.000E+00	1.338E-07	6.792E+00	2.561E-01
2.099E-02	1.777E-03	2.000E+00	2.676E-07	5.817E+00	2.798E-01
2.261E-02	1.626E-03	3.000E+00	4.014E-07	5.272E+00	3.015E-01
2.412E-02	1.506E-03	4.000E+00	5.352E-07	4.893E+00	3.216E-01
2.544E-02	1.325E-03	5.000E+00	6.690E-07	4.514E+00	3.393E-01
2.665E-02	1.204E-03	6.000E+00	8.028E-07	4.191E+00	3.553E-01
2.773E-02	1.084E-03	7.000E+00	9.366E-07	3.898E+00	3.698E-01
2.873E-02	9.937E-04	8.000E+00	1.070E-06	3.641E+00	3.830E-01
2.972E-02	9.937E-04	9.000E+00	1.204E-06	3.464E+00	3.963E-01
3.059E-02	8.732E-04	1.000E+01	1.338E-06	3.271E+00	4.079E-01
3.138E-02	7.829E-04	1.100E+01	1.472E-06	3.082E+00	4.183E-01
3.216E-02	7.829E-04	1.200E+01	1.606E-06	2.936E+00	4.288E-01
3.291E-02	7.528E-04	1.300E+01	1.739E-06	2.809E+00	4.388E-01
3.375E-02	8.431E-04	1.400E+01	1.873E-06	2.743E+00	4.501E-01

Table B.17: Run 7; Jet Height = 7 .5 cm; Test duration = 60 s

Radius (m)	Spacing(m)	Fringe Number (N)	Height(m)	Tau(Pa)	R/H
2.623E-02			0.000E+00		3.497E-01
2.692E-02	6.840E-04	1.000E+00	1.338E-07	4.040E+00	3.589E-01
2.763E-02	7.182E-04	2.000E+00	2.676E-07	4.268E+00	3.684E-01
2.821E-02	5.814E-04	3.000E+00	4.014E-07	3.817E+00	3.762E-01
2.883E-02	6.156E-04	4.000E+00	5.352E-07	3.711E+00	3.844E-01
2.945E-02	6.156E-04	5.000E+00	6.690E-07	3.661E+00	3.926E-01
2.999E-02	5.472E-04	6.000E+00	8.028E-07	3.507E+00	3.999E-01
3.054E-02	5.472E-04	7.000E+00	9.366E-07	3.407E+00	4.072E-01
3.105E-02	5.130E-04	8.000E+00	1.070E-06	3.293E+00	4.140E-01
3.157E-02	5.130E-04	9.000E+00	1.204E-06	3.211E+00	4.209E-01
3.205E-02	4.788E-04	1.000E+01	1.338E-06	3.113E+00	4.273E-01
3.252E-02	4.788E-04	1.100E+01	1.472E-06	3.039E+00	4.337E-01
3.293E-02	4.104E-04	1.200E+01	1.606E-06	2.919E+00	4.391E-01
3.338E-02	4.446E-04	1.300E+01	1.739E-06	2.851E+00	4.451E-01
3.382E-02	4.446E-04	1.400E+01	1.873E-06	2.797E+00	4.510E-01
3.423E-02	4.104E-04	1.500E+01	2.007E-06	2.728E+00	4.565E-01
3.464E-02	4.104E-04	1.600E+01	2.141E-06	2.671E+00	4.619E-01
3.502E-02	3.762E-04	1.700E+01	2.275E-06	2.601E+00	4.669E-01
3.540E-02	3.762E-04	1.800E+01	2.408E-06	2.542E+00	4.720E-01
3.581E-02	4.104E-04	1.900E+01	2.542E-06	2.510E+00	4.774E-01
3.615E-02	3.420E-04	2.000E+01	2.676E-06	2.447E+00	4.820E-01
3.649E-02	3.420E-04	2.100E+01	2.810E-06	2.391E+00	4.865E-01
3.687E-02	3.762E-04	2.200E+01	2.944E-06	2.359E+00	4.916E-01

Table B.18: Run 8; Jet Height = 7 .5 cm; Test duration = 120 s

Radius (m)	Spacing(m)	Fringe Number (N)	Height(m)	Tau(Pa)	R/H
2.633E-02			0.000E+00		3.511E-01
2.756E-02	1.231E-03	1.000E+00	1.338E-07	3.568E+00	3.675E-01
2.890E-02	1.334E-03	2.000E+00	2.676E-07	3.819E+00	3.853E-01
2.999E-02	1.094E-03	3.000E+00	4.014E-07	3.459E+00	3.999E-01
3.109E-02	1.094E-03	4.000E+00	5.352E-07	3.309E+00	4.145E-01
3.201E-02	9.234E-04	5.000E+00	6.690E-07	3.052E+00	4.268E-01
3.297E-02	9.576E-04	6.000E+00	8.028E-07	2.934E+00	4.396E-01
3.382E-02	8.550E-04	7.000E+00	9.366E-07	2.784E+00	4.510E-01
3.461E-02	7.866E-04	8.000E+00	1.070E-06	2.639E+00	4.615E-01
3.536E-02	7.524E-04	9.000E+00	1.204E-06	2.516E+00	4.715E-01
3.611E-02	7.524E-04	1.000E+01	1.338E-06	2.426E+00	4.815E-01
3.676E-02	6.498E-04	1.100E+01	1.472E-06	2.310E+00	4.902E-01
3.752E-02	7.524E-04	1.200E+01	1.606E-06	2.264E+00	5.002E-01
3.813E-02	6.156E-04	1.300E+01	1.739E-06	2.174E+00	5.084E-01
3.871E-02	5.814E-04	1.400E+01	1.873E-06	2.089E+00	5.162E-01
3.933E-02	6.156E-04	1.500E+01	2.007E-06	2.030E+00	5.244E-01
3.995E-02	6.156E-04	1.600E+01	2.141E-06	1.982E+00	5.326E-01
4.049E-02	5.472E-04	1.700E+01	2.275E-06	1.921E+00	5.399E-01
4.104E-02	5.472E-04	1.800E+01	2.408E-06	1.870E+00	5.472E-01
4.155E-02	5.130E-04	1.900E+01	2.542E-06	1.817E+00	5.540E-01
4.203E-02	4.788E-04	2.000E+01	2.676E-06	1.762E+00	5.604E-01
4.254E-02	5.130E-04	2.100E+01	2.810E-06	1.724E+00	5.673E-01
4.302E-02	4.788E-04	2.200E+01	2.944E-06	1.682E+00	5.736E-01

Table B.19: Run 9; Jet Height = 7 .5 cm; Test duration = 180 s

Radius (m)	Spacing(m)	Fringe Number (N)	Height(m)	Tau(Pa)	R/H
4.715E-02			0.000E+00		6.286E-01
4.769E-02	5.470E-04	1.000E+00	1.338E-07	1.194E+00	6.359E-01
4.831E-02	6.154E-04	2.000E+00	2.676E-07	1.207E+00	6.441E-01
4.889E-02	5.812E-04	3.000E+00	4.014E-07	1.171E+00	6.519E-01
4.947E-02	5.812E-04	4.000E+00	5.352E-07	1.158E+00	6.596E-01
5.002E-02	5.470E-04	5.000E+00	6.690E-07	1.127E+00	6.669E-01
5.056E-02	5.470E-04	6.000E+00	8.028E-07	1.109E+00	6.742E-01
5.108E-02	5.128E-04	7.000E+00	9.366E-07	1.079E+00	6.810E-01
5.159E-02	5.128E-04	8.000E+00	1.070E-06	1.059E+00	6.879E-01
5.210E-02	5.128E-04	9.000E+00	1.204E-06	1.045E+00	6.947E-01
5.262E-02	5.128E-04	1.000E+01	1.338E-06	1.036E+00	7.015E-01
5.306E-02	4.444E-04	1.100E+01	1.472E-06	1.005E+00	7.075E-01
5.354E-02	4.786E-04	1.200E+01	1.606E-06	9.914E-01	7.138E-01
5.395E-02	4.103E-04	1.300E+01	1.739E-06	9.608E-01	7.193E-01
5.443E-02	4.786E-04	1.400E+01	1.873E-06	9.541E-01	7.257E-01
5.487E-02	4.444E-04	1.500E+01	2.007E-06	9.403E-01	7.316E-01
5.528E-02	4.103E-04	1.600E+01	2.141E-06	9.208E-01	7.371E-01
5.573E-02	4.444E-04	1.700E+01	2.275E-06	9.119E-01	7.430E-01
5.610E-02	3.761E-04	1.800E+01	2.408E-06	8.901E-01	7.480E-01
5.651E-02	4.103E-04	1.900E+01	2.542E-06	8.779E-01	7.535E-01
5.689E-02	3.761E-04	2.000E+01	2.676E-06	8.611E-01	7.585E-01
5.726E-02	3.761E-04	2.100E+01	2.810E-06	8.462E-01	7.635E-01
5.768E-02	4.103E-04	2.200E+01	2.944E-06	8.389E-01	7.690E-01
5.809E-02	4.103E-04	2.300E+01	3.077E-06	8.326E-01	7.745E-01

Table B.20: Run 9; Jet Height = 7 .5 cm; Test duration = 220 s

Radius (m)	Spacing(m)	Fringe Number (N)	Height(m)	Tau(Pa)	R/H
6.494E-02			0.000E+00		8.658E-01
6.535E-02	4.101E-04	1.000E+00	1.338E-07	6.933E-01	8.713E-01
6.572E-02	3.759E-04	2.000E+00	2.676E-07	6.451E-01	8.763E-01
6.610E-02	3.759E-04	3.000E+00	4.014E-07	6.308E-01	8.813E-01
6.647E-02	3.759E-04	4.000E+00	5.352E-07	6.248E-01	8.863E-01
6.685E-02	3.759E-04	5.000E+00	6.690E-07	6.220E-01	8.913E-01
6.722E-02	3.759E-04	6.000E+00	8.028E-07	6.208E-01	8.963E-01
6.757E-02	3.418E-04	7.000E+00	9.366E-07	6.046E-01	9.009E-01
6.791E-02	3.418E-04	8.000E+00	1.070E-06	5.930E-01	9.054E-01
6.825E-02	3.418E-04	9.000E+00	1.204E-06	5.844E-01	9.100E-01
6.863E-02	3.759E-04	1.000E+01	1.338E-06	5.889E-01	9.150E-01
6.897E-02	3.418E-04	1.100E+01	1.472E-06	5.829E-01	9.196E-01
6.931E-02	3.418E-04	1.200E+01	1.606E-06	5.782E-01	9.241E-01
6.965E-02	3.418E-04	1.300E+01	1.739E-06	5.745E-01	9.287E-01
6.996E-02	3.076E-04	1.400E+01	1.873E-06	5.637E-01	9.328E-01
7.030E-02	3.418E-04	1.500E+01	2.007E-06	5.619E-01	9.373E-01
7.061E-02	3.076E-04	1.600E+01	2.141E-06	5.537E-01	9.414E-01
7.092E-02	3.076E-04	1.700E+01	2.275E-06	5.466E-01	9.455E-01
7.122E-02	3.076E-04	1.800E+01	2.408E-06	5.405E-01	9.496E-01
7.157E-02	3.418E-04	1.900E+01	2.542E-06	5.410E-01	9.542E-01
7.187E-02	3.076E-04	2.000E+01	2.676E-06	5.360E-01	9.583E-01
7.215E-02	2.734E-04	2.100E+01	2.810E-06	5.266E-01	9.620E-01
7.245E-02	3.076E-04	2.200E+01	2.944E-06	5.231E-01	9.661E-01
7.273E-02	2.734E-04	2.300E+01	3.077E-06	5.153E-01	9.697E-01
7.307E-02	3.418E-04	2.400E+01	3.211E-06	5.172E-01	9.743E-01
7.338E-02	3.076E-04	2.500E+01	3.345E-06	5.148E-01	9.784E-01

Table B.21: Run 10; Jet Height = 7 .5 cm; Test duration = 300 s

Radius (m)	Spacing(m)	Fringe Number (N)	Height(m)	Tau(Pa)	R/H
8.458E-02			0.000E+00		1.128E+00
8.495E-02	3.762E-04	1.000E+00	1.338E-07	4.033E-01	1.133E+00
8.533E-02	3.762E-04	2.000E+00	2.676E-07	4.606E-01	1.138E+00
8.564E-02	3.078E-04	3.000E+00	4.014E-07	4.218E-01	1.142E+00
8.594E-02	3.078E-04	4.000E+00	5.352E-07	4.034E-01	1.146E+00
8.625E-02	3.078E-04	5.000E+00	6.690E-07	3.929E-01	1.150E+00
8.656E-02	3.078E-04	6.000E+00	8.028E-07	3.862E-01	1.154E+00
8.687E-02	3.078E-04	7.000E+00	9.366E-07	3.817E-01	1.158E+00
8.721E-02	3.420E-04	8.000E+00	1.070E-06	3.889E-01	1.163E+00
8.748E-02	2.736E-04	9.000E+00	1.204E-06	3.764E-01	1.166E+00
8.779E-02	3.078E-04	1.000E+01	1.338E-06	3.747E-01	1.171E+00
8.810E-02	3.078E-04	1.100E+01	1.472E-06	3.735E-01	1.175E+00
8.841E-02	3.078E-04	1.200E+01	1.606E-06	3.727E-01	1.179E+00
8.871E-02	3.078E-04	1.300E+01	1.739E-06	3.721E-01	1.183E+00
8.899E-02	2.736E-04	1.400E+01	1.873E-06	3.659E-01	1.187E+00
8.930E-02	3.078E-04	1.500E+01	2.007E-06	3.661E-01	1.191E+00
8.960E-02	3.078E-04	1.600E+01	2.141E-06	3.663E-01	1.195E+00
8.988E-02	2.736E-04	1.700E+01	2.275E-06	3.618E-01	1.198E+00
9.015E-02	2.736E-04	1.800E+01	2.408E-06	3.579E-01	1.202E+00
9.042E-02	2.736E-04	1.900E+01	2.542E-06	3.545E-01	1.206E+00
9.070E-02	2.736E-04	2.000E+01	2.676E-06	3.515E-01	1.209E+00
9.097E-02	2.736E-04	2.100E+01	2.810E-06	3.489E-01	1.213E+00
9.124E-02	2.736E-04	2.200E+01	2.944E-06	3.466E-01	1.217E+00
9.152E-02	2.736E-04	2.300E+01	3.077E-06	3.445E-01	1.220E+00
9.183E-02	3.078E-04	2.400E+01	3.211E-06	3.460E-01	1.224E+00
9.207E-02	2.394E-04	2.500E+01	3.345E-06	3.410E-01	1.228E+00

Table B.22: Run 11; Jet Height = 6 cm; Test duration = 50 s

Radius (m)	Spacing(m)	Fringe Number (N)	Height(m)	Tau(Pa)	R/H
2.648E-03			0.000E+00		4.413E-02
6.110E-03	3.462E-03	1.000E+00	1.338E-07	2.232E+01	1.018E-01
9.504E-03	3.394E-03	2.000E+00	2.676E-07	1.920E+01	1.584E-01
1.215E-02	2.648E-03	3.000E+00	4.014E-07	1.650E+01	2.025E-01
1.392E-02	1.765E-03	4.000E+00	5.352E-07	1.353E+01	2.320E-01
1.551E-02	1.595E-03	5.000E+00	6.690E-07	1.181E+01	2.585E-01
1.694E-02	1.426E-03	6.000E+00	8.028E-07	1.061E+01	2.823E-01
1.823E-02	1.290E-03	7.000E+00	9.366E-07	9.709E+00	3.038E-01
1.945E-02	1.222E-03	8.000E+00	1.070E-06	9.052E+00	3.242E-01
2.037E-02	9.165E-04	9.000E+00	1.204E-06	8.242E+00	3.394E-01
2.122E-02	8.486E-04	1.000E+01	1.338E-06	7.583E+00	3.536E-01
2.220E-02	9.844E-04	1.100E+01	1.472E-06	7.233E+00	3.700E-01

Table B.23: Run 12; Jet Height = 6 cm; Test duration = 40 s

Radius (m)	Spacing(m)	Fringe Number (N)	Height(m)	Tau(Pa)	R/H
5.126E-03			0.000E+00		8.543E-02
7.671E-03	2.546E-03	1.000E+00	1.338E-07	1.994E+01	1.279E-01
1.015E-02	2.478E-03	2.000E+00	2.676E-07	1.887E+01	1.692E-01
1.205E-02	1.901E-03	3.000E+00	4.014E-07	1.621E+01	2.008E-01
1.365E-02	1.595E-03	4.000E+00	5.352E-07	1.421E+01	2.274E-01
1.500E-02	1.358E-03	5.000E+00	6.690E-07	1.262E+01	2.501E-01
1.626E-02	1.256E-03	6.000E+00	8.028E-07	1.153E+01	2.710E-01
1.741E-02	1.154E-03	7.000E+00	9.366E-07	1.068E+01	2.902E-01
1.833E-02	9.165E-04	8.000E+00	1.070E-06	9.728E+00	3.055E-01
1.928E-02	9.504E-04	9.000E+00	1.204E-06	9.120E+00	3.213E-01
2.013E-02	8.486E-04	1.000E+01	1.338E-06	8.549E+00	3.355E-01
2.091E-02	7.807E-04	1.100E+01	1.472E-06	8.041E+00	3.485E-01
2.172E-02	8.147E-04	1.200E+01	1.606E-06	7.698E+00	3.621E-01
2.230E-02	5.771E-04	1.300E+01	1.739E-06	7.175E+00	3.717E-01
2.308E-02	7.807E-04	1.400E+01	1.873E-06	6.963E+00	3.847E-01

Table B.24: Run 13; Jet Height = 6 cm; Test duration = 60 s

Radius (m)	Spacing(m)	Fringe Number (N)	Height(m)	Tau(Pa)	R/H
4.444E-03			0.000E+00		7.406E-02
7.870E-03	3.426E-03	1.000E+00	1.338E-07	1.917E+01	1.312E-01
1.109E-02	3.223E-03	2.000E+00	2.676E-07	1.596E+01	1.849E-01
1.343E-02	2.341E-03	3.000E+00	4.014E-07	1.308E+01	2.239E-01
1.526E-02	1.832E-03	4.000E+00	5.352E-07	1.107E+01	2.544E-01
1.686E-02	1.594E-03	5.000E+00	6.690E-07	9.756E+00	2.810E-01
1.825E-02	1.391E-03	6.000E+00	8.028E-07	8.756E+00	3.042E-01
1.947E-02	1.221E-03	7.000E+00	9.366E-07	7.943E+00	3.245E-01
2.059E-02	1.119E-03	8.000E+00	1.070E-06	7.307E+00	3.432E-01
2.154E-02	9.498E-04	9.000E+00	1.204E-06	6.707E+00	3.590E-01
2.246E-02	9.159E-04	1.000E+01	1.338E-06	6.253E+00	3.743E-01
2.317E-02	7.123E-04	1.100E+01	1.472E-06	5.752E+00	3.861E-01

Table B.25: Run 13; Jet Height = 6 cm; Test duration = 90 s

Radius (m)	Spacing(m)	Fringe Number (N)	Height(m)	Tau(Pa)	R/H
4.953E-03			0.000E+00		8.254E-02
9.498E-03	4.545E-03	1.000E+00	1.338E-07	1.510E+01	1.583E-01
1.336E-02	3.867E-03	2.000E+00	2.676E-07	1.287E+01	2.227E-01
1.601E-02	2.646E-03	3.000E+00	4.014E-07	1.025E+01	2.668E-01
1.825E-02	2.239E-03	4.000E+00	5.352E-07	8.783E+00	3.042E-01
1.998E-02	1.730E-03	5.000E+00	6.690E-07	7.554E+00	3.330E-01
2.154E-02	1.560E-03	6.000E+00	8.028E-07	6.736E+00	3.590E-01
2.280E-02	1.255E-03	7.000E+00	9.366E-07	5.996E+00	3.799E-01
2.398E-02	1.187E-03	8.000E+00	1.070E-06	5.466E+00	3.997E-01
2.507E-02	1.085E-03	9.000E+00	1.204E-06	5.040E+00	4.178E-01
2.598E-02	9.159E-04	1.000E+01	1.338E-06	4.633E+00	4.331E-01
2.700E-02	1.018E-03	1.100E+01	1.472E-06	4.389E+00	4.500E-01
2.788E-02	8.820E-04	1.200E+01	1.606E-06	4.139E+00	4.647E-01
2.856E-02	6.784E-04	1.300E+01	1.739E-06	3.847E+00	4.760E-01
2.941E-02	8.480E-04	1.400E+01	1.873E-06	3.688E+00	4.902E-01
3.019E-02	7.802E-04	1.500E+01	2.007E-06	3.534E+00	5.032E-01

Table B.26: Run 14; Jet Height = 6 cm; Test duration = 160 s

Radius (m)	Spacing(m)	Fringe Number (N)	Height(m)	Tau(Pa)	R/H
4.142E-02			0.000E+00		6.903E-01
4.189E-02	4.749E-04	1.000E+00	1.338E-07	1.066E+00	6.982E-01
4.264E-02	7.463E-04	2.000E+00	2.676E-07	1.435E+00	7.107E-01
4.339E-02	7.463E-04	3.000E+00	4.014E-07	1.565E+00	7.231E-01
4.400E-02	6.106E-04	4.000E+00	5.352E-07	1.478E+00	7.333E-01
4.464E-02	6.445E-04	5.000E+00	6.690E-07	1.459E+00	7.440E-01
4.532E-02	6.784E-04	6.000E+00	8.028E-07	1.472E+00	7.553E-01
4.586E-02	5.427E-04	7.000E+00	9.366E-07	1.398E+00	7.644E-01
4.647E-02	6.106E-04	8.000E+00	1.070E-06	1.382E+00	7.745E-01
4.705E-02	5.767E-04	9.000E+00	1.204E-06	1.355E+00	7.841E-01
4.756E-02	5.088E-04	1.000E+01	1.338E-06	1.306E+00	7.926E-01
4.810E-02	5.427E-04	1.100E+01	1.472E-06	1.281E+00	8.017E-01
4.864E-02	5.427E-04	1.200E+01	1.606E-06	1.262E+00	8.107E-01
4.908E-02	4.410E-04	1.300E+01	1.739E-06	1.214E+00	8.181E-01
4.959E-02	5.088E-04	1.400E+01	1.873E-06	1.195E+00	8.265E-01
5.010E-02	5.088E-04	1.500E+01	2.007E-06	1.179E+00	8.350E-01
5.058E-02	4.749E-04	1.600E+01	2.141E-06	1.158E+00	8.429E-01
5.102E-02	4.410E-04	1.700E+01	2.275E-06	1.133E+00	8.503E-01
5.139E-02	3.731E-04	1.800E+01	2.408E-06	1.095E+00	8.565E-01

Table B.27: Run 15; Jet Height = 6 cm; Test duration = 200 s

Radius (m)	Spacing(m)	Fringe Number (N)	Height(m)	Tau(Pa)	R/H
5.818E-02			0.000E+00		9.696E-01
5.865E-02	4.749E-04	1.000E+00	1.338E-07	8.183E-01	9.775E-01
5.916E-02	5.088E-04	2.000E+00	2.676E-07	9.179E-01	9.860E-01
5.957E-02	4.071E-04	3.000E+00	4.014E-07	8.284E-01	9.928E-01
5.997E-02	4.071E-04	4.000E+00	5.352E-07	7.875E-01	9.995E-01
6.041E-02	4.410E-04	5.000E+00	6.690E-07	7.894E-01	1.007E+00
6.079E-02	3.731E-04	6.000E+00	8.028E-07	7.519E-01	1.013E+00
6.123E-02	4.410E-04	7.000E+00	9.366E-07	7.610E-01	1.020E+00
6.160E-02	3.731E-04	8.000E+00	1.070E-06	7.387E-01	1.027E+00
6.197E-02	3.731E-04	9.000E+00	1.204E-06	7.224E-01	1.033E+00
6.238E-02	4.071E-04	1.000E+01	1.338E-06	7.223E-01	1.040E+00
6.275E-02	3.731E-04	1.100E+01	1.472E-06	7.120E-01	1.046E+00
6.313E-02	3.731E-04	1.200E+01	1.606E-06	7.042E-01	1.052E+00
6.347E-02	3.392E-04	1.300E+01	1.739E-06	6.889E-01	1.058E+00
6.377E-02	3.053E-04	1.400E+01	1.873E-06	6.679E-01	1.063E+00

Table B.28: Run 16; Jet Height = 6 cm; Test duration = 380 s

Radius (m)	Spacing(m)	Fringe Number (N)	Height(m)	Tau(Pa)	R/H
9.407E-02			0.000E+00		1.568E+00
9.437E-02	3.051E-04	1.000E+00	1.338E-07	2.826E-01	1.573E+00
9.468E-02	3.051E-04	2.000E+00	2.676E-07	3.042E-01	1.578E+00
9.495E-02	2.712E-04	3.000E+00	4.014E-07	2.886E-01	1.582E+00
9.522E-02	2.712E-04	4.000E+00	5.352E-07	2.810E-01	1.587E+00
9.549E-02	2.712E-04	5.000E+00	6.690E-07	2.767E-01	1.592E+00
9.580E-02	3.051E-04	6.000E+00	8.028E-07	2.852E-01	1.597E+00
9.607E-02	2.712E-04	7.000E+00	9.366E-07	2.817E-01	1.601E+00
9.631E-02	2.373E-04	8.000E+00	1.070E-06	2.708E-01	1.605E+00
9.661E-02	3.051E-04	9.000E+00	1.204E-06	2.774E-01	1.610E+00
9.688E-02	2.712E-04	1.000E+01	1.338E-06	2.760E-01	1.615E+00
9.715E-02	2.712E-04	1.100E+01	1.472E-06	2.749E-01	1.619E+00
9.739E-02	2.373E-04	1.200E+01	1.606E-06	2.685E-01	1.623E+00
9.766E-02	2.712E-04	1.300E+01	1.739E-06	2.683E-01	1.628E+00
9.793E-02	2.712E-04	1.400E+01	1.873E-06	2.681E-01	1.632E+00
9.820E-02	2.712E-04	1.500E+01	2.007E-06	2.681E-01	1.637E+00
9.844E-02	2.373E-04	1.600E+01	2.141E-06	2.639E-01	1.641E+00
9.871E-02	2.712E-04	1.700E+01	2.275E-06	2.642E-01	1.645E+00
9.895E-02	2.373E-04	1.800E+01	2.408E-06	2.608E-01	1.649E+00
9.922E-02	2.712E-04	1.900E+01	2.542E-06	2.613E-01	1.654E+00
9.946E-02	2.373E-04	2.000E+01	2.676E-06	2.585E-01	1.658E+00
9.973E-02	2.712E-04	2.100E+01	2.810E-06	2.591E-01	1.662E+00
9.997E-02	2.373E-04	2.200E+01	2.944E-06	2.567E-01	1.666E+00
1.002E-01	2.373E-04	2.300E+01	3.077E-06	2.546E-01	1.670E+00
1.004E-01	2.373E-04	2.400E+01	3.211E-06	2.527E-01	1.674E+00
1.007E-01	2.373E-04	2.500E+01	3.345E-06	2.509E-01	1.678E+00
1.009E-01	2.373E-04	2.600E+01	3.479E-06	2.493E-01	1.682E+00
1.012E-01	2.712E-04	2.700E+01	3.613E-06	2.503E-01	1.686E+00
1.015E-01	2.712E-04	2.800E+01	3.746E-06	2.513E-01	1.691E+00
1.017E-01	2.373E-04	2.900E+01	3.880E-06	2.499E-01	1.695E+00
1.019E-01	2.373E-04	3.000E+01	4.014E-06	2.487E-01	1.699E+00
1.021E-01	2.034E-04	3.100E+01	4.148E-06	2.454E-01	1.702E+00
1.024E-01	2.373E-04	3.200E+01	4.282E-06	2.444E-01	1.706E+00
1.026E-01	2.373E-04	3.300E+01	4.415E-06	2.436E-01	1.710E+00
1.028E-01	2.034E-04	3.400E+01	4.549E-06	2.408E-01	1.714E+00
1.031E-01	2.373E-04	3.500E+01	4.683E-06	2.401E-01	1.718E+00
1.033E-01	2.373E-04	3.600E+01	4.817E-06	2.395E-01	1.721E+00
1.035E-01	2.373E-04	3.700E+01	4.951E-06	2.389E-01	1.725E+00
1.038E-01	2.373E-04	3.800E+01	5.084E-06	2.384E-01	1.729E+00

Table B.29: Run 17; Jet Height = 6 cm; Test duration = 340 s

Radius (m)	Spacing(m)	Fringe Number (N)	Height(m)	Tau(Pa)	R/H
7.959E-02			0.000E+00		1.327E+00
7.997E-02	3.729E-04	1.000E+00	1.338E-07	4.308E-01	1.333E+00
8.034E-02	3.729E-04	2.000E+00	2.676E-07	4.213E-01	1.339E+00
8.068E-02	3.390E-04	3.000E+00	4.014E-07	3.937E-01	1.345E+00
8.102E-02	3.390E-04	4.000E+00	5.352E-07	3.805E-01	1.350E+00
8.142E-02	4.068E-04	5.000E+00	6.690E-07	4.020E-01	1.357E+00
8.176E-02	3.390E-04	6.000E+00	8.028E-07	3.921E-01	1.363E+00
8.210E-02	3.390E-04	7.000E+00	9.366E-07	3.852E-01	1.368E+00
8.244E-02	3.390E-04	8.000E+00	1.070E-06	3.802E-01	1.374E+00
8.278E-02	3.390E-04	9.000E+00	1.204E-06	3.764E-01	1.380E+00
8.312E-02	3.390E-04	1.000E+01	1.338E-06	3.736E-01	1.385E+00
8.346E-02	3.390E-04	1.100E+01	1.472E-06	3.713E-01	1.391E+00
8.380E-02	3.390E-04	1.200E+01	1.606E-06	3.696E-01	1.397E+00
8.414E-02	3.390E-04	1.300E+01	1.739E-06	3.682E-01	1.402E+00
8.451E-02	3.729E-04	1.400E+01	1.873E-06	3.722E-01	1.408E+00
8.481E-02	3.051E-04	1.500E+01	2.007E-06	3.662E-01	1.414E+00
8.512E-02	3.051E-04	1.600E+01	2.141E-06	3.610E-01	1.419E+00
8.542E-02	3.051E-04	1.700E+01	2.275E-06	3.565E-01	1.424E+00
8.576E-02	3.390E-04	1.800E+01	2.408E-06	3.565E-01	1.429E+00
8.610E-02	3.390E-04	1.900E+01	2.542E-06	3.566E-01	1.435E+00
8.641E-02	3.051E-04	2.000E+01	2.676E-06	3.532E-01	1.440E+00
8.671E-02	3.051E-04	2.100E+01	2.810E-06	3.502E-01	1.445E+00
8.702E-02	3.051E-04	2.200E+01	2.944E-06	3.475E-01	1.450E+00

APPENDIX C: Sonic Nozzle-Exit Data

Table C.1: Run 1; Jet Height = 16.5 cm; Test duration = 20 s

Radius (m)	Spacing(m)	Fringe Number (N)	Height(m)	Tau(Pa)	R/H
1.358E-02			0.000E+00		8.360E-02
1.454E-02	9.575E-04	1.000E+00	1.338E-07	1.835E+01	8.949E-02
1.592E-02	1.376E-03	2.000E+00	2.676E-07	2.269E+01	9.796E-02
1.765E-02	1.735E-03	3.000E+00	4.014E-07	2.605E+01	1.086E-01
1.915E-02	1.496E-03	4.000E+00	5.352E-07	2.502E+01	1.178E-01
2.077E-02	1.616E-03	5.000E+00	6.690E-07	2.502E+01	1.278E-01
2.220E-02	1.436E-03	6.000E+00	8.028E-07	2.406E+01	1.366E-01
2.373E-02	1.526E-03	7.000E+00	9.366E-07	2.372E+01	1.460E-01
2.501E-02	1.287E-03	8.000E+00	1.070E-06	2.261E+01	1.539E-01

Table C.2: Run 2; Jet Height = 16.5 cm; Test duration = 15 s

Radius (m)	Spacing(m)	Fringe Number (N)	Height(m)	Tau(Pa)	R/H
1.345E-02			0.000E+00		8.275E-02
1.423E-02	7.788E-04	1.000E+00	1.338E-07	1.923E+01	8.755E-02
1.519E-02	9.605E-04	2.000E+00	2.676E-07	2.189E+01	9.346E-02
1.628E-02	1.090E-03	3.000E+00	4.014E-07	2.353E+01	1.002E-01
1.755E-02	1.272E-03	4.000E+00	5.352E-07	2.542E+01	1.080E-01
1.877E-02	1.220E-03	5.000E+00	6.690E-07	2.561E+01	1.155E-01
1.989E-02	1.116E-03	6.000E+00	8.028E-07	2.489E+01	1.224E-01
2.095E-02	1.064E-03	7.000E+00	9.366E-07	2.409E+01	1.289E-01
2.217E-02	1.220E-03	8.000E+00	1.070E-06	2.426E+01	1.364E-01

Table C.3: Run 3; Jet Height = 16.5 cm; Test duration = 10 s

Radius (m)	Spacing(m)	Fringe Number (N)	Height(m)	Tau(Pa)	R/H
2.378E-02			0.000E+00		1.441E-01
2.465E-02	8.696E-04	1.000E+00	1.338E-07	2.579E+01	1.494E-01
2.543E-02	7.796E-04	2.000E+00	2.676E-07	2.384E+01	1.541E-01
2.615E-02	7.196E-04	3.000E+00	4.014E-07	2.229E+01	1.585E-01
2.687E-02	7.196E-04	4.000E+00	5.352E-07	2.164E+01	1.628E-01
2.759E-02	7.196E-04	5.000E+00	6.690E-07	2.130E+01	1.672E-01
2.828E-02	6.897E-04	6.000E+00	8.028E-07	2.081E+01	1.714E-01
2.891E-02	6.297E-04	7.000E+00	9.366E-07	1.999E+01	1.752E-01
2.963E-02	7.196E-04	8.000E+00	1.070E-06	2.001E+01	1.795E-01
3.025E-02	6.297E-04	9.000E+00	1.204E-06	1.946E+01	1.834E-01
3.094E-02	6.897E-04	1.000E+01	1.338E-06	1.936E+01	1.875E-01
3.157E-02	6.297E-04	1.100E+01	1.472E-06	1.899E+01	1.914E-01
3.214E-02	5.697E-04	1.200E+01	1.606E-06	1.842E+01	1.948E-01
3.274E-02	5.997E-04	1.300E+01	1.739E-06	1.809E+01	1.984E-01

Table C.4: Run 4; Jet Height = 16.5 cm; Test duration = 20 s

Radius (m)	Spacing(m)	Fringe Number (N)	Height(m)	Tau(Pa)	R/H
2.378E-02			0.000E+00		1.441E-01
2.534E-02	1.559E-03	1.000E+00	1.338E-07	2.513E+01	1.536E-01
2.675E-02	1.409E-03	2.000E+00	2.676E-07	2.298E+01	1.621E-01
2.813E-02	1.379E-03	3.000E+00	4.014E-07	2.204E+01	1.705E-01
2.948E-02	1.349E-03	4.000E+00	5.352E-07	2.141E+01	1.786E-01
3.073E-02	1.259E-03	5.000E+00	6.690E-07	2.054E+01	1.863E-01
3.190E-02	1.169E-03	6.000E+00	8.028E-07	1.955E+01	1.934E-01
3.313E-02	1.229E-03	7.000E+00	9.366E-07	1.913E+01	2.008E-01
3.430E-02	1.169E-03	8.000E+00	1.070E-06	1.863E+01	2.079E-01
3.535E-02	1.049E-03	9.000E+00	1.204E-06	1.789E+01	2.143E-01
3.634E-02	9.895E-04	1.000E+01	1.338E-06	1.716E+01	2.203E-01
3.730E-02	9.595E-04	1.100E+01	1.472E-06	1.655E+01	2.261E-01
3.811E-02	8.096E-04	1.200E+01	1.606E-06	1.573E+01	2.310E-01

Table C.5: Run 5; Jet Height = 16.5 cm; Test duration = 5 s

Radius (m)	Spacing(m)	Fringe Number (N)	Height(m)	Tau(Pa)	R/H
6.987E-03			0.000E+00		4.235E-02
7.468E-03	4.808E-04	1.000E+00	1.338E-07	2.912E+01	4.526E-02
7.821E-03	3.526E-04	2.000E+00	2.676E-07	2.308E+01	4.740E-02
8.173E-03	3.526E-04	3.000E+00	4.014E-07	2.133E+01	4.953E-02
8.590E-03	4.167E-04	4.000E+00	5.352E-07	2.217E+01	5.206E-02
9.038E-03	4.487E-04	5.000E+00	6.690E-07	2.318E+01	5.478E-02
9.487E-03	4.487E-04	6.000E+00	8.028E-07	2.359E+01	5.750E-02
9.968E-03	4.808E-04	7.000E+00	9.366E-07	2.412E+01	6.041E-02
1.048E-02	5.128E-04	8.000E+00	1.070E-06	2.470E+01	6.352E-02
1.106E-02	5.769E-04	9.000E+00	1.204E-06	2.569E+01	6.702E-02
1.157E-02	5.128E-04	1.000E+01	1.338E-06	2.571E+01	7.012E-02
1.208E-02	5.128E-04	1.100E+01	1.472E-06	2.567E+01	7.323E-02

Table C.6: Run 5; Jet Height = 16.5 cm; Test duration = 10 s

Radius (m)	Spacing(m)	Fringe Number (N)	Height(m)	Tau(Pa)	R/H
7.083E-03			0.000E+00		4.293E-02
7.788E-03	7.051E-04	1.000E+00	1.338E-07	2.237E+01	4.720E-02
8.558E-03	7.692E-04	2.000E+00	2.676E-07	2.363E+01	5.186E-02
9.359E-03	8.013E-04	3.000E+00	4.014E-07	2.385E+01	5.672E-02
1.032E-02	9.615E-04	4.000E+00	5.352E-07	2.559E+01	6.255E-02
1.128E-02	9.615E-04	5.000E+00	6.690E-07	2.603E+01	6.838E-02
1.240E-02	1.122E-03	6.000E+00	8.028E-07	2.734E+01	7.517E-02
1.349E-02	1.090E-03	7.000E+00	9.366E-07	2.772E+01	8.178E-02
1.481E-02	1.314E-03	8.000E+00	1.070E-06	2.917E+01	8.974E-02

Table C.7: Run 6; Jet Height = 16.5 cm; Test duration = 10 s

Radius (m)	Spacing(m)	Fringe Number (N)	Height(m)	Tau(Pa)	R/H
1.149E-02			0.000E+00		6.963E-02
1.223E-02	7.381E-04	1.000E+00	1.338E-07	2.653E+01	7.410E-02
1.303E-02	8.023E-04	2.000E+00	2.676E-07	2.775E+01	7.897E-02
1.383E-02	8.023E-04	3.000E+00	4.014E-07	2.751E+01	8.383E-02
1.470E-02	8.665E-04	4.000E+00	5.352E-07	2.803E+01	8.908E-02
1.560E-02	8.986E-04	5.000E+00	6.690E-07	2.842E+01	9.453E-02
1.650E-02	8.986E-04	6.000E+00	8.028E-07	2.845E+01	9.997E-02
1.739E-02	8.986E-04	7.000E+00	9.366E-07	2.832E+01	1.054E-01
1.829E-02	8.986E-04	8.000E+00	1.070E-06	2.813E+01	1.109E-01
1.913E-02	8.344E-04	9.000E+00	1.204E-06	2.753E+01	1.159E-01

Table C.8: Run 6; Jet Height = 16.5 cm; Test duration = 15 s

Radius (m)	Spacing(m)	Fringe Number (N)	Height(m)	Tau(Pa)	R/H
1.159E-02			0.000E+00		7.021E-02
1.255E-02	9.628E-04	1.000E+00	1.338E-07	2.350E+01	7.605E-02
1.383E-02	1.284E-03	2.000E+00	2.676E-07	2.822E+01	8.383E-02
1.502E-02	1.187E-03	3.000E+00	4.014E-07	2.703E+01	9.103E-02
1.643E-02	1.412E-03	4.000E+00	5.352E-07	2.833E+01	9.958E-02
1.765E-02	1.220E-03	5.000E+00	6.690E-07	2.727E+01	1.070E-01
1.897E-02	1.316E-03	6.000E+00	8.028E-07	2.708E+01	1.149E-01
2.041E-02	1.444E-03	7.000E+00	9.366E-07	2.753E+01	1.237E-01
2.160E-02	1.187E-03	8.000E+00	1.070E-06	2.652E+01	1.309E-01
2.263E-02	1.027E-03	9.000E+00	1.204E-06	2.512E+01	1.371E-01

Table C.9: Run 7; Jet Height = 16.5 cm; Test duration = 10 s

Radius (m)	Spacing(m)	Fringe Number (N)	Height(m)	Tau(Pa)	R/H
1.730E-02			0.000E+00		1.048E-01
1.832E-02	1.027E-03	1.000E+00	1.338E-07	3.500E+01	1.111E-01
1.909E-02	7.702E-04	2.000E+00	2.676E-07	2.905E+01	1.157E-01
1.983E-02	7.381E-04	3.000E+00	4.014E-07	2.688E+01	1.202E-01
2.067E-02	8.344E-04	4.000E+00	5.352E-07	2.753E+01	1.253E-01
2.141E-02	7.381E-04	5.000E+00	6.690E-07	2.657E+01	1.297E-01
2.221E-02	8.023E-04	6.000E+00	8.028E-07	2.657E+01	1.346E-01
2.298E-02	7.702E-04	7.000E+00	9.366E-07	2.620E+01	1.393E-01
2.375E-02	7.702E-04	8.000E+00	1.070E-06	2.588E+01	1.439E-01
2.452E-02	7.702E-04	9.000E+00	1.204E-06	2.560E+01	1.486E-01
2.522E-02	7.060E-04	1.000E+01	1.338E-06	2.497E+01	1.529E-01
2.599E-02	7.702E-04	1.100E+01	1.472E-06	2.483E+01	1.575E-01
2.667E-02	6.739E-04	1.200E+01	1.606E-06	2.421E+01	1.616E-01

Table C.10: Run 8; Jet Height = 16.5 cm; Test duration = 35 s

Radius (m)	Spacing(m)	Fringe Number (N)	Height(m)	Tau(Pa)	R/H
7.516E-02			0.000E+00		4.555E-01
7.577E-02	6.098E-04	1.000E+00	1.338E-07	6.395E+00	4.592E-01
7.628E-02	5.135E-04	2.000E+00	2.676E-07	5.647E+00	4.623E-01
7.683E-02	5.456E-04	3.000E+00	4.014E-07	5.648E+00	4.656E-01
7.734E-02	5.135E-04	4.000E+00	5.352E-07	5.499E+00	4.687E-01
7.786E-02	5.135E-04	5.000E+00	6.690E-07	5.423E+00	4.719E-01
7.837E-02	5.135E-04	6.000E+00	8.028E-07	5.382E+00	4.750E-01
7.879E-02	4.172E-04	7.000E+00	9.366E-07	5.081E+00	4.775E-01
7.936E-02	5.777E-04	8.000E+00	1.070E-06	5.271E+00	4.810E-01
7.981E-02	4.493E-04	9.000E+00	1.204E-06	5.133E+00	4.837E-01
8.020E-02	3.851E-04	1.000E+01	1.338E-06	4.899E+00	4.861E-01
8.068E-02	4.814E-04	1.100E+01	1.472E-06	4.889E+00	4.890E-01
8.116E-02	4.814E-04	1.200E+01	1.606E-06	4.884E+00	4.919E-01
8.161E-02	4.493E-04	1.300E+01	1.739E-06	4.834E+00	4.946E-01
8.200E-02	3.851E-04	1.400E+01	1.873E-06	4.702E+00	4.969E-01
8.245E-02	4.493E-04	1.500E+01	2.007E-06	4.677E+00	4.997E-01

Table C.11: Run 8; Jet Height = 16.5 cm; Test duration = 40 s

Radius (m)	Spacing(m)	Fringe Number (N)	Height(m)	Tau(Pa)	R/H
7.503E-02			0.000E+00		4.547E-01
7.583E-02	8.023E-04	1.000E+00	1.338E-07	7.000E+00	4.596E-01
7.648E-02	6.418E-04	2.000E+00	2.676E-07	6.308E+00	4.635E-01
7.705E-02	5.777E-04	3.000E+00	4.014E-07	5.722E+00	4.670E-01
7.760E-02	5.456E-04	4.000E+00	5.352E-07	5.318E+00	4.703E-01
7.815E-02	5.456E-04	5.000E+00	6.690E-07	5.095E+00	4.736E-01
7.875E-02	6.098E-04	6.000E+00	8.028E-07	5.143E+00	4.773E-01
7.936E-02	6.098E-04	7.000E+00	9.366E-07	5.189E+00	4.810E-01
7.985E-02	4.814E-04	8.000E+00	1.070E-06	4.953E+00	4.839E-01
8.039E-02	5.456E-04	9.000E+00	1.204E-06	4.901E+00	4.872E-01
8.094E-02	5.456E-04	1.000E+01	1.338E-06	4.866E+00	4.905E-01
8.145E-02	5.135E-04	1.100E+01	1.472E-06	4.793E+00	4.936E-01
8.193E-02	4.814E-04	1.200E+01	1.606E-06	4.690E+00	4.966E-01
8.238E-02	4.493E-04	1.300E+01	1.739E-06	4.565E+00	4.993E-01

Table C.12: Run 9; Jet Height = 16.5 cm; Test duration = 30 s

Radius (m)	Spacing(m)	Fringe Number (N)	Height(m)	Tau(Pa)	R/H
7.677E-02			0.000E+00		4.653E-01
7.735E-02	5.835E-04	1.000E+00	1.338E-07	7.133E+00	4.688E-01
7.783E-02	4.741E-04	2.000E+00	2.676E-07	6.299E+00	4.717E-01
7.826E-02	4.376E-04	3.000E+00	4.014E-07	5.752E+00	4.743E-01
7.874E-02	4.741E-04	4.000E+00	5.352E-07	5.713E+00	4.772E-01
7.921E-02	4.741E-04	5.000E+00	6.690E-07	5.699E+00	4.801E-01
7.972E-02	5.106E-04	6.000E+00	8.028E-07	5.844E+00	4.832E-01
8.012E-02	4.012E-04	7.000E+00	9.366E-07	5.577E+00	4.856E-01
8.056E-02	4.376E-04	8.000E+00	1.070E-06	5.493E+00	4.883E-01
8.096E-02	4.012E-04	9.000E+00	1.204E-06	5.337E+00	4.907E-01
8.140E-02	4.376E-04	1.000E+01	1.338E-06	5.302E+00	4.933E-01
8.184E-02	4.376E-04	1.100E+01	1.472E-06	5.278E+00	4.960E-01
8.228E-02	4.376E-04	1.200E+01	1.606E-06	5.260E+00	4.986E-01
8.271E-02	4.376E-04	1.300E+01	1.739E-06	5.249E+00	5.013E-01
8.311E-02	4.012E-04	1.400E+01	1.873E-06	5.180E+00	5.037E-01
8.352E-02	4.012E-04	1.500E+01	2.007E-06	5.122E+00	5.062E-01
8.388E-02	3.647E-04	1.600E+01	2.141E-06	5.021E+00	5.084E-01
8.425E-02	3.647E-04	1.700E+01	2.275E-06	4.934E+00	5.106E-01

Table C.13: Run 9; Jet Height = 16.5 cm; Test duration = 60 s

Radius (m)	Spacing(m)	Fringe Number (N)	Height(m)	Tau(Pa)	R/H
7.684E-02			0.000E+00		4.657E-01
7.772E-02	8.753E-04	1.000E+00	1.338E-07	5.233E+00	4.710E-01
7.870E-02	9.847E-04	2.000E+00	2.676E-07	5.751E+00	4.770E-01
7.950E-02	8.023E-04	3.000E+00	4.014E-07	5.219E+00	4.818E-01
8.045E-02	9.482E-04	4.000E+00	5.352E-07	5.406E+00	4.876E-01
8.122E-02	7.659E-04	5.000E+00	6.690E-07	5.097E+00	4.922E-01
8.206E-02	8.388E-04	6.000E+00	8.028E-07	5.047E+00	4.973E-01
8.301E-02	9.482E-04	7.000E+00	9.366E-07	5.206E+00	5.031E-01
8.366E-02	6.565E-04	8.000E+00	1.070E-06	4.899E+00	5.070E-01
8.443E-02	7.659E-04	9.000E+00	1.204E-06	4.811E+00	5.117E-01
8.519E-02	7.659E-04	1.000E+01	1.338E-06	4.746E+00	5.163E-01
8.589E-02	6.929E-04	1.100E+01	1.472E-06	4.621E+00	5.205E-01
8.651E-02	6.200E-04	1.200E+01	1.606E-06	4.451E+00	5.243E-01
8.738E-02	8.753E-04	1.300E+01	1.739E-06	4.537E+00	5.296E-01
8.807E-02	6.929E-04	1.400E+01	1.873E-06	4.464E+00	5.338E-01
8.869E-02	6.200E-04	1.500E+01	2.007E-06	4.348E+00	5.375E-01
8.939E-02	6.929E-04	1.600E+01	2.141E-06	4.301E+00	5.417E-01

Table C.14: Run 10; Jet Height = 16.5 cm; Test duration = 20 s

Radius (m)	Spacing(m)	Fringe Number (N)	Height(m)	Tau(Pa)	R/H
5.457E-02			0.000E+00		3.307E-01
5.533E-02	7.620E-04	1.000E+00	1.338E-07	1.313E+01	3.354E-01
5.595E-02	6.168E-04	2.000E+00	2.676E-07	1.201E+01	3.391E-01
5.653E-02	5.806E-04	3.000E+00	4.014E-07	1.124E+01	3.426E-01
5.711E-02	5.806E-04	4.000E+00	5.352E-07	1.091E+01	3.461E-01
5.769E-02	5.806E-04	5.000E+00	6.690E-07	1.073E+01	3.497E-01
5.824E-02	5.443E-04	6.000E+00	8.028E-07	1.043E+01	3.529E-01
5.874E-02	5.080E-04	7.000E+00	9.366E-07	1.005E+01	3.560E-01
5.929E-02	5.443E-04	8.000E+00	1.070E-06	9.936E+00	3.593E-01
5.980E-02	5.080E-04	9.000E+00	1.204E-06	9.722E+00	3.624E-01
6.027E-02	4.717E-04	1.000E+01	1.338E-06	9.437E+00	3.653E-01
6.081E-02	5.443E-04	1.100E+01	1.472E-06	9.444E+00	3.686E-01
6.128E-02	4.717E-04	1.200E+01	1.606E-06	9.248E+00	3.714E-01
6.176E-02	4.717E-04	1.300E+01	1.739E-06	9.091E+00	3.743E-01
6.223E-02	4.717E-04	1.400E+01	1.873E-06	8.963E+00	3.771E-01
6.270E-02	4.717E-04	1.500E+01	2.007E-06	8.859E+00	3.800E-01
6.313E-02	4.354E-04	1.600E+01	2.141E-06	8.695E+00	3.826E-01

Table C.15: Run 11; Jet Height = 16.5 cm; Test duration = 80 s

Radius (m)	Spacing(m)	Fringe Number (N)	Height(m)	Tau(Pa)	R/H
1.123E-01			0.000E+00		6.803E-01
1.129E-01	6.519E-04	1.000E+00	1.338E-07	3.280E+00	6.843E-01
1.134E-01	5.215E-04	2.000E+00	2.676E-07	2.615E+00	6.874E-01
1.140E-01	6.084E-04	3.000E+00	4.014E-07	2.669E+00	6.911E-01
1.147E-01	6.519E-04	4.000E+00	5.352E-07	2.801E+00	6.951E-01
1.152E-01	4.781E-04	5.000E+00	6.690E-07	2.569E+00	6.980E-01
1.157E-01	5.650E-04	6.000E+00	8.028E-07	2.549E+00	7.014E-01
1.163E-01	5.650E-04	7.000E+00	9.366E-07	2.537E+00	7.048E-01
1.169E-01	5.650E-04	8.000E+00	1.070E-06	2.530E+00	7.083E-01
1.176E-01	6.953E-04	9.000E+00	1.204E-06	2.658E+00	7.125E-01
1.181E-01	5.215E-04	1.000E+01	1.338E-06	2.605E+00	7.156E-01
1.185E-01	4.346E-04	1.100E+01	1.472E-06	2.493E+00	7.183E-01
1.190E-01	5.215E-04	1.200E+01	1.606E-06	2.466E+00	7.214E-01
1.195E-01	4.781E-04	1.300E+01	1.739E-06	2.414E+00	7.243E-01
1.200E-01	5.215E-04	1.400E+01	1.873E-06	2.399E+00	7.275E-01
1.206E-01	5.215E-04	1.500E+01	2.007E-06	2.387E+00	7.306E-01

Table C.16: Run 12; Jet Height = 12 cm; Test duration = 5 s

Radius (m)	Spacing(m)	Fringe Number (N)	Height(m)	Tau(Pa)	R/H
3.507E-03			0.000E+00		2.922E-02
3.889E-03	3.825E-04	1.000E+00	1.338E-07	2.814E+01	3.241E-02
4.272E-03	3.825E-04	2.000E+00	2.676E-07	2.665E+01	3.560E-02
4.750E-03	4.782E-04	3.000E+00	4.014E-07	2.917E+01	3.958E-02
5.292E-03	5.419E-04	4.000E+00	5.352E-07	3.134E+01	4.410E-02
5.929E-03	6.376E-04	5.000E+00	6.690E-07	3.390E+01	4.941E-02
6.790E-03	8.607E-04	6.000E+00	8.028E-07	3.870E+01	5.658E-02

Table C.17: Run 13; Jet Height = 12 cm; Test duration = 5 s

Radius (m)	Spacing(m)	Fringe Number (N)	Height(m)	Tau(Pa)	R/H
7.906E-03			0.000E+00		6.588E-02
8.320E-03	4.144E-04	1.000E+00	1.338E-07	2.961E+01	6.933E-02
8.894E-03	5.738E-04	2.000E+00	2.676E-07	3.667E+01	7.412E-02
9.531E-03	6.376E-04	3.000E+00	4.014E-07	4.036E+01	7.943E-02
1.030E-02	7.651E-04	4.000E+00	5.352E-07	4.509E+01	8.580E-02
1.097E-02	6.694E-04	5.000E+00	6.690E-07	4.435E+01	9.138E-02
1.176E-02	7.969E-04	6.000E+00	8.028E-07	4.582E+01	9.802E-02
1.262E-02	8.607E-04	7.000E+00	9.366E-07	4.748E+01	1.052E-01

Table C.18: Run 13; Jet Height = 12 cm; Test duration = 15 s

Radius (m)	Spacing(m)	Fringe Number (N)	Height(m)	Tau(Pa)	R/H
7.778E-03			0.000E+00		6.482E-02
9.404E-03	1.626E-03	1.000E+00	1.338E-07	3.727E+01	7.837E-02
1.157E-02	2.168E-03	2.000E+00	2.676E-07	4.330E+01	9.643E-02
1.409E-02	2.518E-03	3.000E+00	4.014E-07	4.741E+01	1.174E-01
1.639E-02	2.295E-03	4.000E+00	5.352E-07	4.600E+01	1.365E-01
1.855E-02	2.168E-03	5.000E+00	6.690E-07	4.395E+01	1.546E-01
2.037E-02	1.817E-03	6.000E+00	8.028E-07	4.065E+01	1.697E-01
2.219E-02	1.817E-03	7.000E+00	9.366E-07	3.866E+01	1.849E-01

Table C.19: Run 14; Jet Height = 12 cm; Test duration = 5 s

Radius (m)	Spacing(m)	Fringe Number (N)	Height(m)	Tau(Pa)	R/H
1.001E-02			0.000E+00		8.341E-02
1.068E-02	6.694E-04	1.000E+00	1.338E-07	4.867E+01	8.899E-02
1.135E-02	6.694E-04	2.000E+00	2.676E-07	4.864E+01	9.457E-02
1.192E-02	5.738E-04	3.000E+00	4.014E-07	4.340E+01	9.935E-02
1.262E-02	7.013E-04	4.000E+00	5.352E-07	4.459E+01	1.052E-01
1.336E-02	7.332E-04	5.000E+00	6.690E-07	4.578E+01	1.113E-01
1.396E-02	6.057E-04	6.000E+00	8.028E-07	4.365E+01	1.164E-01
1.470E-02	7.332E-04	7.000E+00	9.366E-07	4.435E+01	1.225E-01
1.530E-02	6.057E-04	8.000E+00	1.070E-06	4.285E+01	1.275E-01
1.588E-02	5.738E-04	9.000E+00	1.204E-06	4.128E+01	1.323E-01

Table C.20: Run 14; Jet Height = 12 cm; Test duration = 15 s

Radius (m)	Spacing(m)	Fringe Number (N)	Height(m)	Tau(Pa)	R/H
1.001E-02			0.000E+00		8.341E-02
1.189E-02	1.881E-03	1.000E+00	1.338E-07	4.248E+01	9.909E-02
1.409E-02	2.200E-03	2.000E+00	2.676E-07	4.668E+01	1.174E-01
1.600E-02	1.913E-03	3.000E+00	4.014E-07	4.298E+01	1.334E-01
1.792E-02	1.913E-03	4.000E+00	5.352E-07	4.086E+01	1.493E-01
1.980E-02	1.881E-03	5.000E+00	6.690E-07	3.930E+01	1.650E-01
2.174E-02	1.945E-03	6.000E+00	8.028E-07	3.875E+01	1.812E-01
2.321E-02	1.466E-03	7.000E+00	9.366E-07	3.589E+01	1.934E-01

APPENDIX D: Particle Removal Data

Table D.1a: Summary of particle removal data

R (mm)	H (mm)	R/H	Pulse	MPS (Diameters)	Particles Before	Particles After	Removal Efficiency
75	150	0.5	0.02	13.9	55	15	0.72727273
75	150	0.5	0.02	11.3	57	18	0.68421053
75	150	0.5	0.02	10.1	89	25	0.71910112
75	150	0.5	0.02	13.9	45	14	0.68888889
75	150	0.5	0.02	10.7	82	35	0.57317073
75	150	0.5	0.02	19.6	24	14	0.41666667
75	150	0.5	0.02	15.1	59	28	0.52542373
75	150	0.5	0.02	11.9	70	33	0.52857143
75	150	0.5	0.02	15.8	45	22	0.51111111
75	150	0.5	0.02	13.5	58	17	0.70689655
75	150	0.5	0.02	14.6	50	25	0.5
75	150	0.5	0.02	18.1	31	14	0.5483871
75	150	0.5	0.02	13.9	50	15	0.7
75	150	0.5	0.02	19.2	32	13	0.59375
75	150	0.5	0.02	14.7	49	24	0.51020408
75	150	0.5	0.02	20.8	28	10	0.64285714
75	150	0.5	0.02	16.3	28	13	0.53571429
75	150	0.5	0.02	18.7	38	17	0.55263158
75	150	0.5	0.02	13.2	45	19	0.57777778
75	150	0.5	0.02	15.6	45	22	0.51111111
112.5	150	0.75	0.02	18.7	26	23	0.11538462
112.5	150	0.75	0.02	12.5	48	46	0.04166667
112.5	150	0.75	0.02	12.7	62	56	0.09677419
112.5	150	0.75	0.02	12.2	55	53	0.03636364
112.5	150	0.75	0.02	10.5	80	80	0
112.5	150	0.75	0.02	18.8	43	42	0.02325581
112.5	150	0.75	0.02	11.2	70	68	0.02857143
112.5	150	0.75	0.02	12.4	54	53	0.01851852
112.5	150	0.75	0.02	11.9	60	58	0.03333333
112.5	150	0.75	0.02	15.9	43	42	0.02325581
90	150	0.6	0.02	12.3	53	31	0.41509434
90	150	0.6	0.02	17.7	42	28	0.33333333
90	150	0.6	0.02	14.5	52	31	0.40384615
90	150	0.6	0.02	16.2	43	25	0.41860465
90	150	0.6	0.02	11.3	91	72	0.20879121
90	150	0.6	0.02	14.1	51	27	0.47058824

Table D.1b: Continuation of Table D.1

R (mm)	H (mm)	R/H	Pulse	MPS (Diameters)	Particles Before	Particles After	Removal Efficiency
90	150	0.6	0.02	18.5	35	20	0.42857143
90	150	0.6	0.02	13.9	55	29	0.47272727
90	150	0.6	0.02	10.2	77	38	0.50649351
90	150	0.6	0.02	11.2	66	46	0.3030303
60	150	0.4	0.02	12.1	75	20	0.73333333
60	150	0.4	0.02	11.2	89	13	0.85393258
60	150	0.4	0.02	12.9	49	15	0.69387755
60	150	0.4	0.02	12.7	62	32	0.48387097
60	150	0.4	0.02	17	39	9	0.76923077
60	150	0.4	0.02	14.4	61	26	0.57377049
60	150	0.4	0.02	12.2	67	23	0.65671642
60	150	0.4	0.02	14.5	50	18	0.64
60	150	0.4	0.02	16	47	21	0.55319149
60	150	0.4	0.02	11.4	79	36	0.5443038
30	150	0.2	0.02	15.7	51	16	0.68627451
30	150	0.2	0.02	10.8	68	24	0.64705882
30	150	0.2	0.02	14	53	17	0.67924528
30	150	0.2	0.02	11	85	18	0.78823529
30	150	0.2	0.02	11.7	92	30	0.67391304
30	150	0.2	0.02	12.9	75	11	0.85333333
30	150	0.2	0.02	12.6	57	13	0.77192982
30	150	0.2	0.02	10.7	96	22	0.77083333
30	150	0.2	0.02	11.2	94	11	0.88297872
30	150	0.2	0.02	11.9	77	20	0.74025974
30	150	0.2	0.02	9.5	101	23	0.77227723
30	150	0.2	0.02	11.1	93	17	0.8172043
30	150	0.2	0.02	10.3	83	26	0.68674699
30	150	0.2	0.02	9.2	138	40	0.71014493
30	150	0.2	0.02	10	100	19	0.81
30	150	0.2	0.02	12.4	54	24	0.55555556
30	150	0.2	0.02	11.3	90	18	0.8
30	150	0.2	0.02	11.3	79	22	0.72151899
30	150	0.2	0.02	9.7	92	29	0.68478261
30	150	0.2	0.02	10.5	89	31	0.65168539
1.5	150	0.01	0.02	11	101	39	0.61386139
1.5	150	0.01	0.02	13.6	57	13	0.77192982
1.5	150	0.01	0.02	14.4	53	15	0.71698113

Table D.1c: Continuation of Table D.1

R (mm)	H (mm)	R/H	Pulse	MPS (Diameters)	Particles Before	Particles After	Removal Efficiency
1.5	150	0.01	0.02	17.2	51	21	0.58823529
1.5	150	0.01	0.02	13.1	54	21	0.61111111
1.5	150	0.01	0.02	10.2	105	34	0.67619048
1.5	150	0.01	0.02	11.3	91	13	0.85714286
1.5	150	0.01	0.02	11.6	85	28	0.67058824
1.5	150	0.01	0.02	11.6	77	33	0.57142857
1.5	150	0.01	0.02	11.2	65	15	0.76923077
15	150	0.1	0.02	13.8	63	17	0.73015873
15	150	0.1	0.02	12.9	57	10	0.8245614
15	150	0.1	0.02	11.4	77	19	0.75324675
15	150	0.1	0.02	15.3	61	7	0.8852459
15	150	0.1	0.02	12.8	68	15	0.77941176
15	150	0.1	0.02	12.8	65	15	0.76923077
15	150	0.1	0.02	12.9	60	7	0.88333333
15	150	0.1	0.02	12.8	58	14	0.75862069
15	150	0.1	0.02	19.3	31	5	0.83870968
15	150	0.1	0.02	14.1	53	13	0.75471698
75	150	0.5	0.02	6.1	280	205	0.26785714
75	150	0.5	0.02	6.5	272	156	0.42647059
75	150	0.5	0.02	6.3	272	115	0.57720588
75	150	0.5	0.02	6	342	255	0.25438596
75	150	0.5	0.02	6.2	315	202	0.35873016
75	150	0.5	0.02	5.6	383	245	0.36031332
75	150	0.5	0.02	6.7	275	194	0.29454545
75	150	0.5	0.02	6	308	264	0.14285714
75	150	0.5	0.02	6.4	238	191	0.19747899
75	150	0.5	0.02	7	218	169	0.22477064

Reference List

[1] Jankowski, P., Mecado A., & Hallowell, S. (1992). FAA Explosive Vapor/Particle Detection Technology. *SPIE, 1824,* 13-24.

[2] Raber, E., Jin, A., Noonan, K., McGuire, R., & Kirvel, R. D. (2001). Decontamionation issues for chemical and biological warfare agents: How clean is clean enough?. *International Journal of Environmental Health Research, 11,* 128-48.

[3] Settles, G. S., (2006). Fluid mechanics and homeland security. *Annual Review Fluid Mechanics, 38,* 87-110.

[4] Settles, G. S., Sniffers: fluid-dynamic smpling for olfactory trace detection in nature and homeland security – The 2004 Freeman Scholar Lecture. *Journal of Fluids Engineering, 127,* 189-218.

[5] Gutfinger, C. & Ziskind, G. (1999). Particle resuspension by air jets-application to clean rooms. *Journal of Aerosol Science, 30,* 537-538.

[6] Chang, Po-Sheng, Brock, J. R., & Trachtenberg, I. (1993). Aerosol jet cleaning of silicon wafer surfaces. *Surface Chemical Cleaning and Passivation for Semiconductor Processing Symposium,* 249-54.

[7] Whyte, W. (2001). *Clean room technology: fundamentals of design, testing, and operation.* New York: Wiley.

[8] Smedley, G. T., Phares, D. J., & Flagan R. C. (1999). Entrainment of fine particle from surfaces by gas jets impinging at a normal incidence. *Experiments in Fluids, 26,* 324-34.

[9] Phares, D. J., Smedley, G. T., & Flagan R. C. (2000). The wall shear stress produced by the normal impingement of a jet on a flat surface. *Journal Fluid Mechanics, 418,* 351-75.

[10] Tanner, L. H. & Blows, L. G. (1976). A study of the motion of oil fils on surfaces in air flow, with the application to the measurement of skin friction. *Journal of Physics E, 9,* 194-202.

[11] Driver, D. M. (2003). Application of oil-film interferometry skin-friction measurement to large wind tunnels. *Experiments in Fluids, 34,* 717-25.

[12] Naughton, J. W. (2005). High-Quality Skin Friction Measurements in 2-D Flows Using Oil Film Interferometry. *21st International Congress on Instrumentation in Aerospace Simulation Facilities, 2005.V,* 166-75.

[13] Ziskind, G., Fichman, M., & Gutfinger, C. (1995). Resuspension of particulates from surfaces to turbulent flows: Review and analysis. *Journal of Aerosol Science,* 26, 613-644.

[14] Ziskind, G. (2006). Particle resuspension from surfaces: Revisited and re-evaluated. *Reviews in Chemical Engineering* 22 (1-2), 1-123.

[15] Nicholson, K. W. (1988). A review of particle resuspension. *Atmospheric Environment,* 22, 2639-2651.

[16] Fromentin, A. (1989). Time dependent particle resuspension from a multi-layer deposit by turbulent flow. *Journal Aerosol Science,* 20, 911-914.

[17] Ibrahim, A. H., Dunn, P.F., & Brach, R. M. (2003). Microparticle detachment from surfaces exposed to turbulent air flow: controlled experiments and modeling. *Journal of Aerosol Science,* 34 (6), 765-782.

[18] Braaten, D. A., Shaw, R. H., & Paw, U. K. T. (1990). Particle resuspension in a turbulent boundary layer. *Journal of Aerosol Science*, 21, 613-628.

[19] Corino, E. R., & Brodkey, R. S. (1969). A visual investigation of the wall region in a turbulent flow. *Journal of Fluid Mechanics*, 37, part 1, 1-30.

[20] Yung, B. P. K., Merry, H., & Bott, T. R. (1989). The role of turbulent bursts in particle re-entrainment in aqueous systems. *Chemical Engineering ScienceI*, 44, 873-882.

[21] Reeks, M. W. & Hall, D. (2001). Kinetic models for particle resuspension in turbulent flows: theory and measurement. *Journal of Aerosol Science,* 32 (1), 1-31.

[22] John, W., Fritter, D. N., & Winklmayr, W. (1991). Resuspension Induced by impacting particles. *Journal of Aerosol Science* 22 (6), 723-736.

[23] Ibrahim, A. H., Dunn, P. F., & Brach, R. M. (2004). Microparticle detachment from surfaces exposed to turbulent air flow: Effects of flow and particle deposition characteristics. *Journal of Aerosol Science,* 35 (7), 805-821.

[24] Smedley, G. T., Phares, D. J., & Flagan R. C. (2001). Entrainment of fine particle from surfaces by gas jets impinging at oblique incidence. *Experiments in Fluids, 30,* 135-422.

[25] Settles, G. S., "Sniffers: fluid-dynamic sampling for olfactory trace detection in nature and homeland security - the 2004 Freeman Scholar Lecture," *Journal of Fluids Engineering*, 127(2):189-218, 2005.

[26] Settles, G. S., Ferree, H. C., Tronosky, M. D., Moyer, Z. M., and McGann, W. J., "Natural aerodynamic portal sampling of trace explosives from the human body," *Proceedings of the 3rd International Symposium on Explosive Detection and Aviation Security*, Federal Aviation Administration, Atlantic City, New Jersey, November 2001.

[27] Braaten, D. A. (1994). Wind-tunnel experiments of large particle reentrainment-deposition and development of large particle scaling parameters. *Aerosol Science and Technology,* 21 (2),157-169.

[28] Ibrahim, A. H. & Dunn, P. F. (2006). Effects of temporal flow acceleration on the detachment of microparticles from surfaces. *Journal of Aerosol Science*, 37 (10),1258-1266.

[29] Ibrahim, A. H., Dunn, P. F., & Qazi, M. F. (2008). Experiments and validation of a model for microparticle detachment from a surface by turbulent air flow. *Journal of Aerosol Science,* 39 (8), 645-656.

[30] Naughton, J. W., & Liu, T. (2007). Photogrammetry in oil-film interferometry. *AIAA Journal, 45,* 1620-29.

[31] Pope, S.B. (2000). *Turbulent Flows,* Cambridge University Press: Cambridge.

[32] Settles, G. S. (2001). *Schlieren and Shadowgraph Techniques,* Springer-Verlag: New York.